

Accepted Manuscript

Biomass segregation between biofilm and flocs improves the control of nitrite-oxidizing bacteria in mainstream partial nitrification and anammox processes

Michele Laureni, David G. Weissbrodt, Kris Villez, Orlane Robin, Nadieh de Jonge, Alex Rosenthal, George Wells, Jeppe Lund Nielsen, Eberhard Morgenroth, Adriano Joss

PII: S0043-1354(19)30001-6

DOI: <https://doi.org/10.1016/j.watres.2018.12.051>

Reference: WR 14347

To appear in: *Water Research*

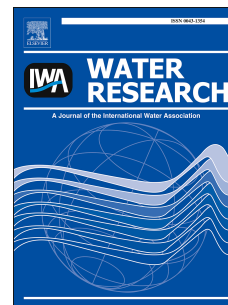
Received Date: 20 October 2018

Revised Date: 24 December 2018

Accepted Date: 27 December 2018

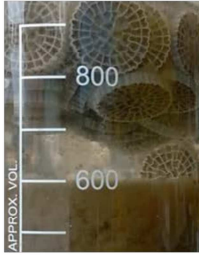
Please cite this article as: Laureni, M., Weissbrodt, D.G., Villez, K., Robin, O., de Jonge, N., Rosenthal, A., Wells, G., Nielsen, J.L., Morgenroth, E., Joss, A., Biomass segregation between biofilm and flocs improves the control of nitrite-oxidizing bacteria in mainstream partial nitrification and anammox processes, *Water Research*, <https://doi.org/10.1016/j.watres.2018.12.051>.

This is a PDF file of an unedited manuscript that has been accepted for publication. As a service to our customers we are providing this early version of the manuscript. The manuscript will undergo copyediting, typesetting, and review of the resulting proof before it is published in its final form. Please note that during the production process errors may be discovered which could affect the content, and all legal disclaimers that apply to the journal pertain.

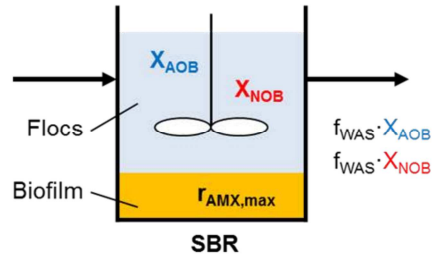


Mainstream PN/A
In hybrid MBBR

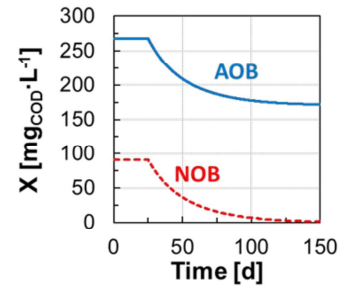
Biomass
segregation



Mathematical
model



Selective NOB
washout



ACCEPTED MANUSCRIPT

1 **Biomass segregation between biofilm and flocs improves the control of**
2 **nitrite-oxidizing bacteria in mainstream partial nitrification and**
3 **anammox processes**

4
5
6 Michele Laureni^{1,2,a,b,*}, David G. Weissbrodt^{3,4}, Kris Villez¹, Orlane Robin¹, Nadieh de Jonge⁴, Alex
7 Rosenthal⁵, George Wells⁵, Jeppe Lund Nielsen⁴, Eberhard Morgenroth^{1,2}, Adriano Joss¹

8 ¹ Eawag: Swiss Federal Institute of Aquatic Science and Technology, Überlandstrasse 133, 8600
9 Dübendorf, Switzerland

10 ² Institute of Environmental Engineering, ETH Zürich, Stefano-Franscini-Platz 5, CH-8093 Zürich,
11 Switzerland

12 ³ Department of Biotechnology, Delft University of Technology, Van der Maasweg 9, NL- 2629 HZ
13 Delft, The Netherlands

14 ⁴ Department of Chemistry and Bioscience, Aalborg University, Fredrik Bajers Vej 7H, DK-9220
15 Aalborg, Denmark

16 ⁵ Northwestern University, Department of Civil and Environmental Engineering, Evanston, IL, USA

17
18 *Corresponding author: Michele Laureni (m.laureni@tudelft.nl, mil@bio.aau.dk)

19
20 ^a Present address: Department of Biotechnology, Delft University of Technology, Van der Maasweg
21 9, NL- 2629 HZ Delft, The Netherlands

22 ^b Present address: Department of Chemistry and Bioscience, Aalborg University, Fredrik Bajers Vej
23 7H, DK-9220 Aalborg, Denmark

24
25
26
27
28
29
30 Submitted to Water Research on 17.10.18

31 *A previous version of the manuscript (WR38690) had been submitted on 24.02.17 for publication in*
32 *Water Research but was rejected on 03.10.17 with invitation to resubmit to Water Research as new*
33 *manuscript.*

34

35 **Abstract**

36 The control of nitrite-oxidizing bacteria (NOB) challenges the implementation of partial nitrification
37 and anammox (PN/A) processes under mainstream conditions. The aim of the present study was to
38 understand how operating conditions impact microbial competition and the control of NOB in hybrid
39 PN/A systems, where biofilm and flocs coexist. A hybrid PN/A moving-bed biofilm reactor (MBBR;
40 also referred to as integrated fixed film activated sludge or IFAS) was operated at 15 °C on
41 aerobically pre-treated municipal wastewater ($23 \text{ mg}_{\text{NH}_4\text{-N}}\cdot\text{L}^{-1}$). Ammonium-oxidizing bacteria
42 (AOB) and NOB were enriched primarily in the flocs, and anammox bacteria (AMX) in the biofilm.
43 After decreasing the dissolved oxygen concentration (DO) from 1.2 to $0.17 \text{ mg}_{\text{O}_2}\cdot\text{L}^{-1}$ - with all other
44 operating conditions unchanged - washout of NOB from the flocs was observed. The activity of the
45 minor NOB fraction remaining in the biofilm was suppressed at low DO. As a result, low effluent
46 NO_3^- concentrations ($0.5 \text{ mg}_{\text{N}}\cdot\text{L}^{-1}$) were consistently achieved at aerobic nitrogen removal rates (80
47 $\text{mg}_{\text{N}}\cdot\text{L}^{-1}\cdot\text{d}^{-1}$) comparable to those of conventional treatment plants. A simple dynamic mathematical
48 model, assuming perfect biomass segregation with AOB and NOB in the flocs and AMX in the
49 biofilm, was able to qualitatively reproduce the selective washout of NOB from the flocs in response
50 to the decrease in DO-setpoint. Similarly, numerical simulations indicated that flocs removal is an
51 effective operational strategy to achieve the selective washout of NOB. The direct competition for
52 NO_2^- between NOB and AMX - the latter retained in the biofilm and acting as a “ NO_2 -sink” - was
53 identified by the model as key mechanism leading to a difference in the actual growth rates of AOB
54 and NOB (*i.e.*, $\mu_{\text{NOB}} < \mu_{\text{AOB}}$ in flocs) and allowing for the selective NOB washout over a broad range
55 of simulated sludge retention times (SRT = 6.8 - 24.5 d). Experimental results and model predictions
56 demonstrate the increased operational flexibility, in terms of variables that can be easily controlled
57 by operators, offered by hybrid systems as compared to solely biofilm systems for the control of
58 NOB in mainstream PN/A applications.

59 **Keywords:** Mainstream anammox; partial nitrification/anammox; hybrid system; IFAS; biomass
60 segregation; NOB washout; mathematical modelling; nitrite sink

ACCEPTED MANUSCRIPT

61 1 Introduction

62 Partial nitrification and anammox (PN/A) is a resource-efficient alternative process for the removal of
63 nitrogen from municipal wastewater (MWW) and holds promise to bring wastewater treatment plants
64 (WWTP) close to neutral or even positive energy balances (Siegrist *et al.*, 2008, van Loosdrecht and
65 Brdjanovic 2014). PN/A technologies are implemented for the treatment of warm and concentrated
66 streams such as digester supernatant (“sidestream PN/A”; Lackner *et al.*, (2014)). Research targeting
67 the direct application of PN/A to more dilute MWW, or “mainstream PN/A”, is progressing at a fast
68 pace (De Clippeleir *et al.*, 2013, Gilbert *et al.*, 2015a, Laurenzi *et al.*, 2016, Lotti *et al.*, 2015). The
69 challenges associated with mainstream PN/A relate to the highly variable, dilute and cold
70 characteristics of MWW. Moreover, mainstream PN/A must guarantee volumetric N-removal rates
71 comparable to conventional WWTP (*i.e.*, $100 \text{ mg}_N \cdot \text{L}^{-1} \cdot \text{d}^{-1}$; Metcalf & Eddy *et al.*, (2013)) and
72 reliably discharge effluent to stringent water quality standards (*e.g.*, below $2 \text{ mg}_{\text{NH}_4\text{-N}} \cdot \text{L}^{-1}$ in
73 Switzerland; WPO (1998)).

74 Successful PN/A relies on the concerted activity of aerobic (AOB) and anaerobic ammonium-
75 oxidizing (AMX) bacteria (Speth *et al.*, 2016). Optimized microbial community engineering
76 strategies are required to favour the growth of AOB and retain the slower-growing AMX, while out-
77 competing the undesired nitrite-oxidizing bacteria (NOB). Several operational strategies
78 implemented in sidestream applications are not feasible under mainstream conditions. At mesophilic
79 temperatures ($> 20^\circ\text{C}$), AOB display higher maximum growth rates than NOB, which allows
80 selective NOB washout at a sufficiently low solids retention time. Conversely, at mainstream
81 temperatures between $10\text{-}20^\circ\text{C}$ (in temperate regions), the differences in growth rates are minimal
82 (Hellings *et al.*, 1998). In addition, nitrogen concentrations in the main line are too low for NOB to
83 be inhibited by free ammonia (NH_3) or free nitrous acid (HNO_2) (Anthonisen *et al.*, 1976, Jubany *et*
84 *al.*, 2009). As a result, NOB control and washout cannot be based on maximum growth rates alone,

85 as is efficiently achieved in sidestream suspended biomass systems (Hellings *et al.*, 1998, Joss *et al.*,
86 2011).

87 The use of biofilms, either grown on carrier material or in the form of granular bio-aggregates, has
88 proven effective to achieve stable and resilient PN/A under mainstream conditions at laboratory scale
89 (Gilbert *et al.*, 2015a, Laureni *et al.*, 2016, Lotti *et al.*, 2015). Biofilms allow for the long solids
90 retention times (SRT) needed to retain AMX, while substrate gradients promote the suppression of
91 NOB activity (Brockmann and Morgenroth 2010, Gilbert *et al.*, 2015a, Laureni *et al.*, 2016, Lotti *et al.*,
92 *et al.*, 2014, Pérez *et al.*, 2014). NOB control in biofilm systems is mainly driven by the competition for
93 oxygen with AOB, with the latter usually featuring higher substrate affinities (Brockmann and
94 Morgenroth 2010, Corbala-Robles *et al.*, 2016, Pérez *et al.*, 2014). PN/A operation under oxygen-
95 limited NH_4^+ oxidation can favour nitrification while limiting the aerobic growth of NOB (Brockmann
96 and Morgenroth 2010, Isanta *et al.*, 2015, Pérez *et al.*, 2014). However, operation under oxygen
97 limitation inherently limits the AOB activity as well, and thus the overall process rate (Laureni *et al.*,
98 2015, Perez *et al.*, 2014). Moreover, despite the generally accepted higher affinity of AOB for
99 oxygen (Rittmann and McCarty 2001), NOB are known to adapt to low dissolved oxygen
100 concentrations (DO) (Liu and Wang 2013), and several studies have recently reported higher oxygen
101 affinities for NOB than AOB (Malovanyy *et al.*, 2015, Regmi *et al.*, 2014, Sliekers *et al.*, 2005).
102 Lastly, although their activity can be suppressed, NOB can persist in the biofilm and become active
103 when favourable conditions are re-established, making their long-term suppression in solely biofilm
104 systems challenging (Fux *et al.*, 2004, Gilbert *et al.*, 2015a, Isanta *et al.*, 2015, Laureni *et al.*, 2016,
105 Lotti *et al.*, 2014).

106 Hybrid systems, where biofilms and flocs coexist (also referred to as integrated fixed film activated
107 sludge or IFAS), are currently receiving increased attention for their potential advantages for PN/A
108 applications. Experimental evidence (Laureni *et al.*, 2016, Leix *et al.*, 2016, Malovanyy *et al.*, 2015,
109 Park *et al.*, 2014, Shi *et al.*, 2016, Veuillet *et al.*, 2014, Vlaeminck *et al.*, 2010, Wells *et al.*, 2017,

110 Winkler *et al.*, 2011) and numerical results (Hubaux *et al.*, 2015, Volcke *et al.*, 2012) indicate that
111 the faster-growing aerobic guilds tend to enrich in the floc fraction, with direct access to dissolved
112 substrates. In turn, AMX have been shown to enrich in the biofilm, where anoxic conditions are
113 achieved. As a result, differential control of the retention times of the bacterial guilds associated with
114 the two biomass fractions is in principle possible (Wett *et al.*, 2015). Moreover, as flocs are less
115 diffusion-limited than biofilms, significantly higher aerobic volumetric conversion rates can be
116 achieved even at low DO (Veillet *et al.*, 2014). Nonetheless, published data on hybrid systems
117 operated for PN/A remain limited and seemingly contradictory. Hybrid systems at high flocs
118 concentrations above $1 \text{ g}_{\text{TSS}} \cdot \text{L}^{-1}$ have been applied at full scale to treat digester supernatant at
119 mesophilic temperatures with negligible NOB activity (Veillet *et al.*, 2014). Conversely, increased
120 NOB activity has been reported in hybrid systems with a fraction of flocs as small as $< 10\%$ of total
121 solids (Hubaux *et al.*, 2015, Laurenzi *et al.*, 2016). The implications of biomass segregation and
122 operational conditions for microbial competition in hybrid systems are as yet largely unknown.

123 The aim of this work was to understand the dominant mechanisms controlling the interaction
124 between biofilm and flocs, the influence of operating conditions, and their implications for NOB
125 control in hybrid PN/A systems. The effect of the DO on NOB was assessed experimentally in an
126 IFAS system operated on real MWW at 15°C . In parallel, a simplified dynamic mathematical model
127 of the hybrid system was developed to provide a mechanistic interpretation of the experimental
128 results, and to understand how the composition of the flocs and the NOB concentration respond to
129 changes in DO, flocs removal, and AMX activity in the biofilm. The sensitivity of the simulation
130 outcome to model parameters was assessed. Relevant scenarios for engineering practice are also
131 discussed.

132 2 Materials and methods

133 2.1 Long-term reactor operation at different DO

134 A 12 L hybrid MBBR was operated as a sequencing batch reactor (SBR) for PN/A on aerobically
135 pre-treated MWW (see next section). The reactor was filled at a volumetric ratio of 33% with K5
136 biofilm carriers (AnoxKaldnes™, Sweden; protected surface of $800 \text{ m}^2 \cdot \text{m}^{-3}$). The biomass was
137 previously acclimatised to the influent for over one year (Laureni *et al.*, 2016). The reactor was run
138 for 565 days at $15.5 \pm 1.0^\circ\text{C}$. Each SBR cycle consisted of six steps: feeding (5 L of pre-treated
139 MWW, 5 min), anoxic mixing (10 min; 200 rpm), aeration and mixing (variable duration in the range
140 60 - 200 min; terminated at a residual NH_4^+ concentration of $2 \text{ mg}_{\text{NH}_4\text{-N}} \cdot \text{L}^{-1}$), anoxic mixing (60 min),
141 settling (60 min), and effluent discharge (terminated at 7 L fill level; 2 min). The DO was varied
142 between micro-aerobic conditions (Phases I, III, V: $0.17 \pm 0.04 \text{ mg}_{\text{O}_2} \cdot \text{L}^{-1}$; (Gilbert *et al.*, 2015b)),
143 and aerobic conditions (Phases II, IV: $1.2 \pm 0.2 \text{ mg}_{\text{O}_2} \cdot \text{L}^{-1}$ and $1.6 \pm 0.1 \text{ mg}_{\text{O}_2} \cdot \text{L}^{-1}$; (Regmi *et al.*,
144 2014)) (Figure 2). The total cycle duration varied between 3.5 ± 0.5 and 5.3 ± 0.3 h for operation at
145 high and low DO, respectively.

146 The reactor was equipped with an optical oxygen sensor (Oxymax COS61D), ion-selective
147 electrodes for NH_4^+ and NO_3^- concentrations, and pH and temperature sensors (ISEmax CAS40D),
148 all from Endress+Hauser (Switzerland). The pH was not controlled and remained stable at 7.4 ± 0.2
149 throughout the experimental period. Operational data are presented in Figure S1.

150 2.2 Municipal wastewater (MWW)

151 The municipal wastewater was taken from the sewer of Dübendorf (Switzerland). After primary
152 treatment (screen, sand removal and primary clarifier), MWW was pre-treated in an aerated 12 L
153 SBR operated for high-rate organic carbon (as COD) removal at an SRT of 1 d. The pre-treated
154 MWW featured the following characteristics: $54 \pm 13 \text{ mg}_{\text{COD}_{\text{sol}}} \cdot \text{L}^{-1}$, $23 \pm 6 \text{ mg}_{\text{NH}_4\text{-N}} \cdot \text{L}^{-1}$, and < 0.3

155 $\text{mg}_\text{N}\cdot\text{L}^{-1}$ of NO_2^- and NO_3^- . Prior to feeding to the PN/A reactor, the pre-treated MWW was stored in
 156 a temperature-controlled ($< 20^\circ\text{C}$) external buffer tank of 50 L to equalize the hydraulic loads.

157 2.3 Control of total suspended solids (TSS) and calculation of their dynamic SRT

158 In addition to the settling step in the SBR cycle, from day 70 onwards the reactor effluent was
 159 filtered through a 10 L filter-bag (50- μm -mesh; 3M™ NB Series, Nylon Monofilament) placed in a
 160 50 L barrel. The content of the net was centrifuged for 5 min at $2000 \times g$, and the solids were
 161 reintroduced into the reactor on a daily basis. The TSS in the reactor and all activities were measured
 162 one cycle after biomass reintroduction.

163 The dynamic total SRT was calculated considering only the observed sludge loss in the effluent and
 164 by sampling (modified from Takács *et al.*, (2008)):

$$165 \quad \text{SRT}_{t+\Delta t} = \text{SRT}_t \cdot \left(1 - \frac{X_{\text{effluent}} \cdot V_{\text{effluent}} + X_{\text{reactor}} \cdot V_{\text{sample}}}{X_{\text{reactor}} \cdot V_{\text{reactor}}} \right) + \Delta t \quad (1)$$

166 where X_{effluent} is the average TSS concentration in the sock-net effluent ($\text{g}_{\text{TSS}}\cdot\text{L}^{-1}$), V_{effluent} is the total
 167 effluent volume discharged during the time interval, V_{sample} is the volume taken out for biomass
 168 sampling, X_{reactor} is the TSS concentration in the reactor ($\text{g}_{\text{TSS}}\cdot\text{L}^{-1}$), V_{reactor} is the volume of the bulk
 169 liquid phase in the reactor (12 L), and Δt is the time interval between subsequent measurements (d).

170 The aerobic SRT is calculated from the total SRT as follows:

$$171 \quad \text{SRT}_{\text{aerobic}} = \text{SRT} \cdot \frac{t_{\text{aerobic}}}{t_{\text{total}}} \quad (2)$$

172 where $t_{\text{aerobic}}/t_{\text{total}}$ is the actual fraction of aerobic time over the total batch time (Figure S1). The
 173 development of TSS, SRT and $\text{SRT}_{\text{aerobic}}$ over time is presented in Figure S2, together with the
 174 volumetric particle size distribution of the flocs measured on days 451 and 465 via laser light
 175 scattering (Mastersizer 2000, Malvern, UK). During the experiment, $\text{SRT}_{\text{aerobic}}$ increased from 4.7 to
 176 49.1 days.

177 **2.4 Maximum activities of AOB, NOB and AMX, and their segregation between biofilm and**
178 **flocs**

179 The maximum anammox activity ($r_{AMX,max}$) is defined as the volumetric rate of nitrogen removal
180 (sum of NH_4^+ and NO_2^-) in the absence of DO and under non-limiting concentrations of NH_4^+ and
181 NO_2^- . $r_{AMX,max}$ was measured *in-situ* once or twice a week. The maximum activities of AOB and
182 NOB ($r_{AOB,max}$ and $r_{NOB,max}$) are defined respectively as the volumetric rates of NH_4^+ oxidation and
183 NO_3^- production. $r_{AOB,max}$ and $r_{NOB,max}$ were measured via *ex-situ* batch tests (1 L) run under fully
184 aerobic conditions ($> 5 \text{ mg}_{O_2}\cdot\text{L}^{-1}$) and non-limiting concentrations of NH_4^+ and NO_2^- . The liquid
185 fraction was sampled during mixing and a proportional number of random carriers were chosen
186 manually. Mixing was provided with a magnetic stirrer (200 rpm) and the temperature was
187 maintained at $15 \pm 1^\circ\text{C}$. After manually removing all carriers, $r_{AOB,max}$ and $r_{NOB,max}$ of the flocs were
188 measured. The $r_{AMX,max}$ value of the suspension was checked *ex-situ* five times throughout the
189 experimental period and was confirmed to be negligible. NH_4^+ and NO_2^- were supplied as NH_4Cl and
190 $NaNO_2$ ($20\text{-}30 \text{ mg}_N\cdot\text{L}^{-1}$), and volumetric consumption rates were calculated by linear regression of
191 laboratory measurements of 3-4 grab samples from the bulk liquid phase.

192 **2.5 Activities of AOB, NOB, and AMX during regular operation (aerobic step)**

193 The volumetric activities of the three main autotrophic guilds during regular operation ($r_{AOB,cycle}$,
194 $r_{NOB,cycle}$ and $r_{AMX,cycle}$ expressed as $\text{mg}_{NH_4-N}\cdot\text{L}^{-1}\cdot\text{d}^{-1}$, $\text{mg}_{NO_3-N}\cdot\text{L}^{-1}\cdot\text{d}^{-1}$, and $\text{mg}_{(NH_4+NO_2)-N}\cdot\text{L}^{-1}\cdot\text{d}^{-1}$
195 respectively) were estimated according to Laurenzi *et al.*, (2016). In short, during the aerated step of
196 an SBR cycle, the consumption of NH_4^+ , accumulation of NO_2^- and production of NO_3^- were
197 followed by laboratory measurements of 3-4 grab samples from the bulk liquid phase. The activities
198 were estimated based on the stoichiometric and kinetic matrix presented in Table 1, with parameters
199 from Table 2. Heterotrophic denitrification during aeration was assumed to be negligible (Laurenzi *et*
200 *al.*, 2016).

201 2.6 Nitrogen removal over the entire SBR cycle and during the aerobic step

202 Over the entire SBR cycle, the volumetric N-removal rate ($\text{mg}_N \cdot \text{L}^{-1} \cdot \text{d}^{-1}$) was calculated by dividing
 203 the difference between the sum of the dissolved nitrogen species (NH_4^+ , NO_2^- and NO_3^-) in the
 204 influent and effluent by the hydraulic retention time (HRT, d). The relative removals (%) of NH_4^+
 205 and total nitrogen are defined as the difference between their influent and effluent concentrations
 206 divided by the influent concentrations. The influent and effluent were sampled once per week (Figure
 207 S3).

208 During aeration, the aerobic volumetric N-removal rate ($\text{mg}_N \cdot \text{L}^{-1} \cdot \text{d}^{-1}$) was calculated as the difference
 209 between the NH_4^+ consumption rate and the rates of NO_2^- and NO_3^- production. The aerobic N-
 210 removal efficiency (%) was estimated by dividing the N-removal rate during aeration by the NH_4^+
 211 depletion rate.

212 2.7 Growth rate of AOB, NOB, and AMX

213 The maximum growth rates of AOB ($\mu_{\text{AOB,max}}$) and NOB ($\mu_{\text{NOB,max}}$) were estimated during *Phase II*,
 214 when substrate limitations were minor, based on the measured exponential increase in their
 215 maximum activity in the flocs ($r_{i,\text{max}}$, Figure 2b), or in their activity during operation ($r_{i,\text{cycle}}$, Figure
 216 2c). Most of the activity increase occurred in suspension, where diffusion limitation was assumed to
 217 be of minor importance. The potential seeding of AOB and NOB from the biofilm was neglected,
 218 possibly resulting in a slight overestimation of $\mu_{i,\text{max}}$. The suspended solids mass balance (X_i , with
 219 $i=\text{AOB, NOB}$) is expressed as:

$$220 \quad \frac{dX_i}{dt} = \left(\mu_{i,\text{max}} - b_i - \frac{1}{\text{SRT}} \right) \cdot X_i = \mu_{i,\text{obs}} \cdot X_i \quad (3)$$

221 where $\mu_{i,\text{max}}$ and $\mu_{i,\text{obs}}$ are the maximum and observed growth rates, respectively, of the guild i (d^{-1}),
 222 b_i is the decay rate of the guild i (d^{-1} ; set to $0.05 \mu_{i,\text{max}}$), and SRT is the solids retention time (d). The
 223 value of $\mu_{i,\text{obs}}$ was obtained from the exponential interpolation of the measured increase in activities
 224 (r_i , $\text{mg}_N \cdot \text{L}^{-1} \cdot \text{d}^{-1}$):

$$r_{i,t} = r_{i,t-\Delta t} \cdot \exp(\mu_{i,obs} \cdot \Delta t) \quad (4).$$

From Eq. 3 and 4, and considering that growth occurs only during the aerobic time, the maximum growth rate can be estimated as follows:

$$\mu_{i,max} = (\mu_{i,obs} + b_i) \cdot \frac{t_{total}}{t_{aerobic}} + \frac{1}{SRT_{aerobic}} \quad (5)$$

where $t_{aerobic}/t_{total}$ is the average fraction of aerobic time over the total batch time, and $SRT_{aerobic}$ the average aerobic SRT during the considered period. The SRT was not considered in the estimation of the maximum growth rate of AMX ($\mu_{AMX,max}$), as their growth occurred almost exclusively on the biofilm. The uncertainty associated with $\mu_{i,max}$ was quantified by means of Monte Carlo simulations as previously described (Laureni *et al.*, 2015).

2.8 Amplicon sequencing analyses of the bacterial community compositions in biofilm and flocs

The amplicon sequencing method is presented in the Supporting Information, Section S1 (Laureni *et al.*, 2016).

2.9 Analytical methods

The concentration of NH_4^+ was analysed using a flow injection analyser (FIAstar 5000, Foss, Denmark). The concentrations of NO_2^- and NO_3^- were analysed by ion chromatography (Compact IC 761, Metrohm, Switzerland). The COD was measured photometrically with test kits (Hach Lange, Germany). The samples were filtered using 0.45 μm filters (Macherey-Nagel, Germany) prior to analysis. The concentration of total and volatile suspended solids (VSS, TSS) in the mixed liquors was determined according to standard methods (APHA 2005). The total solids (TS) on biofilm carriers were estimated as described previously (Laureni *et al.*, 2016).

246 3 Mathematical model of the hybrid system

247 3.1 Model description

248 A dynamic model of the hybrid MBBR operated in SBR mode was developed and implemented in
249 MATLAB (version R2015b, MathWorks Inc.). The MATLAB scripts are available as open-source
250 code in the Supporting Information. The aim of the model was to understand how the composition of
251 the flocs and the NOB concentration respond to changes in DO, fraction of flocs removed per SBR
252 cycle (f_{WAS}), and maximum volumetric AMX activity ($r_{AMX,max}$). To this end, perfect biomass
253 segregation was assumed, with AOB and NOB in the flocs and AMX in the biofilm (Figure 1).

254 Five soluble compounds were considered: ammonium (NH_4^+), nitrite (NO_2^-), nitrate (NO_3^-), di-
255 nitrogen gas (N_2), and DO.

256 The AOB, NOB, and AMX processes were modelled according to the stoichiometric and kinetic
257 matrix in Table 1. Unless explicitly stated, parameter values were taken from the literature (Table 2).
258 X_{AOB} and X_{NOB} were assumed to grow in the flocs, and their abundance and activity to be influenced
259 by growth and washout. For the sake of simplicity, the model excluded decay processes. Free
260 ammonia and free nitrous acid inhibitions were considered negligible under mainstream
261 concentrations and pH.

262 AMX were considered to grow in a deep biofilm (Morgenroth 2008). The primary goal of the
263 modelling was to understand the role of the biofilm as “NO₂-sink”: the biofilm was consequently
264 modelled as zero-dimensional, and spatial gradients were neglected. In order to discuss the potential
265 effects of diffusion, additional simulations were run with 10-fold increased values for NO_2^- and NH_4^+
266 affinity constants of AMX. Moreover, as the activity of deep biofilms is transport-limited rather than
267 biomass-limited, the maximum AMX process rate ($\rho_{AMX,max} = \mu_{AMX,max} \cdot X_{AMX}$, $mg_{COD} \cdot L^{-1} \cdot d^{-1}$; Table
268 1) was assumed to be constant during each simulation. This was implemented by considering the
269 concentration of AMX (X_{AMX}) and the process rate as constants. The oxygen inhibition of AMX was
270 not explicitly modelled: deep biofilms are in fact oxygen-limited, and the modelled AMX activity is

271 to be considered the activity resulting from the anoxic biofilm layers. For consistency with the
272 experimental part, the simulation results are presented as a function of $r_{AMX,max}$ ($mg_{(NH_4+NO_2)-N} \cdot L^{-1} \cdot d^{-1}$)
273 as obtained by the product of $\rho_{AMX,max}$ and the sum of the stoichiometric coefficients for NH_4^+ and
274 NO_2^- (Table 1).

275 3.2 Simulation strategy and scenario analysis

276 The influent was assumed to contain $20 mg_{NH_4-N} \cdot L^{-1}$ and be devoid of NO_2^- , NO_3^- , and COD. Filling,
277 settling, and decanting steps were assumed to be instantaneous. Only the aerated phase was
278 simulated dynamically. As in the operation of the experimental reactor, settling was initiated each
279 time the NH_4^+ concentration equalled $2 mg_N \cdot L^{-1}$; this resulted in variable cycle durations depending
280 on biomass activity. Simulations were performed for a temperature of $15^\circ C$ at which maximum
281 growth rates were estimated in the reactor. The DO was assumed constant, and the volumetric
282 exchange of MWW was 50 % per cycle. The initial concentration of NH_4^+ at the start of each cycle
283 was the result of mixing (half of its value at the end of the previous cycle plus half of the influent
284 concentration, *i.e.*, $11 mg_N \cdot L^{-1}$). The NO_2^- and NO_3^- concentrations at the start of each simulated
285 cycle were always equal to half of their values at the end of the previous cycle. A fixed fraction of
286 flocs (f_{WAS}) was removed at the end of each cycle. f_{WAS} was defined as the mass removed from the
287 reactor divided by mass of solids present in the reactor, $(X_{removed} \cdot V_{removed}) / (X_{reactor} \cdot V_{reactor})$.
288 Simulations were run until a pseudo steady-state was reached, *i.e.*, constant effluent N and flocs
289 concentration. Pseudo steady-state were shown to be independent from the initial X_{AOB} and X_{NOB} .
290 The sensitivity of the model outputs was assessed with respect to the ratio between the O_2 affinity
291 constants of NOB and AOB ($K_{O_2,NOB} / K_{O_2,AOB}$) and the ratio between the NO_2^- affinity constants of
292 NOB and AMX ($K_{NO_2,NOB} / K_{NO_2,AMX}$) (Table S1, Figures S9).

293 A combination of different $\rho_{AMX,max}$ ($0 - 24 mg_{COD} \cdot L^{-1} \cdot d^{-1}$; corresponding to $r_{AMX,max}$ $0-300$
294 $mg_{(NH_4+NO_2)-N} \cdot L^{-1} \cdot d^{-1}$), and f_{WAS} ($0.4 - 1.7\%$) were simulated for two DO (0.15 and $1.5 mg_{O_2} \cdot L^{-1}$).
295 These modelled parameter values were explicitly chosen to fall in the range of the experimental

296 values. To assess the impact of the individual control parameters, four specific scenarios are
 297 discussed (Table 3).

298 3.3 Interdependence between f_{WAS} , HRT, and SRT

299 For an SBR where the reaction phase of the cycle is always extended until the target effluent NH_4^+
 300 concentration is reached ($2 \text{ mg}_N \cdot L^{-1}$), the HRT, the f_{WAS} , and ultimately the SRT are interdependent.
 301 At pseudo steady-state, the AOB removed at the end of each cycle must equal the growth of AOB
 302 during that cycle:

$$303 \quad f_{WAS} \cdot X_{AOB}(T) \cdot V_{reactor} = \int_{\tau=0}^T \mu_{AOB}(\tau) \cdot X_{AOB}(\tau) \cdot V_{reactor} \cdot d\tau \quad (6)$$

304 where $X_{AOB}(T)$ is the concentration of AOB at the end of a cycle ($\text{mg}_{COD} \cdot L^{-1}$), T is the length of the
 305 cycle (d), $V_{reactor}$ is the working volume of the reactor (L), $\mu_{AOB}(\tau)$ is the actual growth rate of AOB
 306 at time τ during the cycle (d^{-1}), and $X_{AOB}(\tau)$ is the AOB concentration at time τ ($\text{mg}_{COD} \cdot L^{-1}$). Under
 307 the simplifying assumption that over a cycle $\mu_{AOB} \approx \text{const.}$ and $X_{AOB} \approx \text{const.}$, Eq. 6 can be simplified
 308 to

$$309 \quad f_{WAS} \approx \mu_{AOB} \cdot T \quad (7).$$

310 From Eq. 7 it can be seen that the HRT and the cycle time are directly linked: for a given actual
 311 growth rate of AOB, increasing f_{WAS} increases T , and thus the HRT. As a result, HRT and f_{WAS}
 312 cannot be controlled independently. The value of f_{WAS} also impacts the pseudo steady-state X_{AOB} and
 313 X_{NOB} , and lower biomass concentrations result from higher f_{WAS} . Furthermore, this has direct
 314 implications on the SRT of the flocs, defined as the average biomass present in the reactor divided by
 315 the biomass removed per cycle. Under the simplifying assumption that $X \approx \text{const.}$ over a cycle, it
 316 follows that

$$317 \quad SRT \approx \frac{X \cdot V_{reactor}}{(f_{WAS} \cdot X \cdot V_{reactor})/T} \approx \frac{T}{f_{WAS}} \approx \frac{1}{\mu_{AOB}} \quad (8)$$

318 From Eq. 8, after substituting Eq. 7, it can be seen that the SRT is not an independent parameter
319 either, but is directly determined by the actual growth rate of the AOB for the given environmental
320 conditions.

ACCEPTED MANUSCRIPT

321 4 Results and Discussion

322 4.1 Long term operation of the hybrid MBBR, and the impact of DO on NOB control

323 4.1.1 Maximum volumetric activities ($r_{i,max}$) segregation between biofilm and flocs

324 A 12-L hybrid MBBR was operated for mainstream PN/A at 15 °C on aerobically pre-treated MWW,
325 and the impact of the DO on microbial competition and NOB control was investigated. The total and
326 flocs-associated maximum volumetric activities ($r_{i,max}$) of the three main guilds were measured as
327 proxy for their abundance (Figures 2a, b).

328 Over more than one year the reactor was stably operated as PN/A (*i.e.* prior to *Phase I* in Fig. 2;
329 (Laureni *et al.*, 2016)). During *Phase II*, as a result of the simultaneous increase in DO from 0.17 to
330 1.2 mg_{O2}·L⁻¹ and the improved flocs retention, $r_{AOB,max}$ and $r_{NOB,max}$ increased exponentially (Figure
331 2b). The observed increase was mainly associated with the flocs (dotted line in Figure 2b). Over the
332 same period, the total suspended solids increased from 0.2 to 1 g_{TSS}·L⁻¹ (Figure S2). The estimated
333 maximum growth rate of AOB ($\mu_{AOB,max}$) and NOB ($\mu_{NOB,max}$) were 0.30 ± 0.06 and 0.34 ± 0.06 d⁻¹,
334 respectively. For AMX, a $\mu_{AMX,max}$ of 0.014 ± 0.004 d⁻¹ was estimated.

335 The increase in $r_{AOB,max}$ and $r_{NOB,max}$ stopped when the DO was decreased to its initial value of 0.17
336 mg_{O2}·L⁻¹ (day 115, *Phase III*) while keeping all other operational conditions unchanged. After an
337 apparent delay of over six weeks, $r_{NOB,max}$ started to decrease while the established $r_{AOB,max}$ was
338 maintained in the system (Figure 2b). The loss in $r_{NOB,max}$ was primarily associated with the flocs.

339 During *Phase IV*, $r_{AOB,max}$ and $r_{NOB,max}$ increased exponentially, in particular when the DO was
340 increased to 1.6 mg_{O2}·L⁻¹ (day 460). Unfortunately, the increase stopped on day 475, when a
341 dramatic drop in all $r_{i,max}$ was observed in correlation with a multiple-day heavy rain event. This also
342 coincided with a 15% loss of TSS in the system, although this alone cannot explain the activity loss.
343 Importantly, all $r_{i,max}$ naturally recovered in less than two months (*Phase V*, Figure 2). All operational
344 conditions are presented in Figure S1.

345 4.1.2 Volumetric activities during regular operation ($r_{i,cycle}$)

346 The actual volumetric activities ($r_{i,cycle}$) of the three main guilds were measured during the aerobic
347 step of an SBR cycle to assess the impact of the imposed operational condition on microbial
348 competition. Actual activities are presented in Figure 2c, and the observed yields of NH_4^+ converted
349 to NO_2^- and NO_3^- are displayed in Figure 2d.

350 During periods of high DO (*Phase II* and *IV*), the volumetric activities during regular operation
351 ($r_{i,cycle}$) were comparable to the maximum activities ($r_{i,max}$), indicating that substrate limitations were
352 minor under these conditions (Figures 2a, c). The $\mu_{AOB,max}$ ($0.28 \pm 0.05 \text{ d}^{-1}$) and $\mu_{NOB,max}$ (0.30 ± 0.06
353 d^{-1}), estimated during *Phase II*, were in good agreement with those obtained from the increase in
354 $r_{i,max}$.

355 Decreasing the DO on day 115 (*Phase III*) resulted in an immediate decrease of $r_{AOB,cycle}$ and
356 $r_{NOB,cycle}$, as both guilds become DO limited (Figure 2c). After a delay of about two months, $r_{NOB,cycle}$
357 started to decrease progressively in accordance with the behaviour of $r_{NOB,max}$. The decrease in
358 $r_{NOB,cycle}$ coincided with the increase of $r_{AMX,cycle}$, indicating a progressive shift in the competition for
359 NO_2^- . From day 285 onwards, very little NOB activity was detected as supported by the low NO_3^-
360 production. The slight NO_2^- accumulation indicated an excess of $r_{AOB,cycle}$ over the available $r_{AMX,cycle}$
361 (Figure 2d).

362 The increase in DO on day 375 (*Phase IV*) led to a sharp increase in $r_{AOB,cycle}$ and lead, due to the
363 excess AOB maintained in the system, to a pronounced accumulation of NO_2^- to about 60% of the
364 consumed NH_4^+ (Figure 2d). The $r_{NOB,cycle}$ also increased immediately, due to the NOB persisting in
365 the biofilm, and NO_3^- started to accumulate. The exponential increase of $r_{AOB,cycle}$ and $r_{NOB,cycle}$
366 stopped on day 475 in conjunction with the heavy rain event (Figure 2c, empty arrow).

367 4.1.3 Bacterial community composition of biofilm and flocs

368 The relative read abundances of AOB, NOB, and AMX in the biofilm and flocs are presented in
369 Figure 3. The dynamics of all individual OTUs detected within the three guilds are shown in Figure

370 S4. In good agreement with the observed $r_{AMX,max}$, AMX were almost exclusively present in the
371 biofilm with relative abundances of up to 15% of the total reads (< 0.1% in suspension).
372 Interestingly, four different OTUs were detected for AMX in the biofilm and displayed different
373 dynamics, suggesting possible fine-scale differentiation in the “*Ca. Brocadia*” lineage. Fluorescence
374 *in situ* hybridization (FISH) micrographs of biofilm cryosections are shown in Figure S7.

375 Significantly lower relative read abundances were observed for AOB and NOB throughout the entire
376 operation (Figures 3b, c). During *Phase III*, the TSS increased from 1 to over 2.5 $g_{TSS}\cdot L^{-1}$ (Figure
377 S2). The relative abundance of AOB (genus *Nitrosomonas*) progressively increased from
378 approximately 0.5 to over 2.5% in the flocs, whereas the relative abundance of NOB (genus
379 *Nitrospira*) decreased progressively from 0.4 to below 0.1%. Thus, the observed loss of NOB
380 activity (Figure 2) coincided with the actual washout of NOB from the flocs. The relative read
381 abundances of both AOB and NOB guilds during *Phase IV* increased markedly on the biofilm,
382 supporting the observed increases in $r_{AOB,max}$ and $r_{NOB,max}$ (Figure 2). Two different OTUs were
383 identified for AOB with distinct trends in biofilm and flocs.

384 The ratio of the relative read abundances of AOB and NOB is shown in Figure 3d. AOB were
385 selectively enriched over NOB in the flocs during the period at low DO (*Phase III*); the AOB/NOB
386 ratio increased from 5 to over 20. No major changes in the AOB/NOB ratio were observed in the
387 biofilm.

388 **4.1.4 NOB control at low DO: wash-out from the flocs and activity suppression in the biofilm**

389 AOB and NOB grew in the flocs and biofilm. The enrichment of both guilds in the flocs, less
390 diffusion-limited, is in good agreement with previous experimental and modelling reports on PN/A
391 (Hubaux *et al.*, 2015, Park *et al.*, 2014, Veuillet *et al.*, 2014, Vlaeminck *et al.*, 2010, Volcke *et al.*,
392 2012, Winkler *et al.*, 2011). Also, AOB and NOB displayed comparable maximum specific growth
393 rates as expected at mainstream temperatures (Hellinga *et al.*, 1998). In principle, these conditions
394 would hinder the possibility to differentiate the actual growth rates of the two guilds and selectively

395 wash out NOB as efficiently achieved in sidestream suspended biomass systems (Hellings *et al.*,
396 1998, Joss *et al.*, 2011). Nevertheless, prolonged operation at low DO ($0.17 \text{ mg}_{\text{O}_2}\cdot\text{L}^{-1}$) did result in
397 the selective wash out of NOB from the flocs (Figure 2). This is explained by a distinctive
398 characteristic of hybrid systems, namely the competition for NO_2^- between the NOB in the flocs and
399 the AMX enriched in the biofilm acting as a “ NO_2^- -sink”. The proposed mechanisms for the selective
400 NOB washout are extensively discussed in the modelling section.

401 The accumulation and persistence of an NOB fraction in biofilms has also been widely reported, and
402 makes the suppression of NO_2^- oxidation challenging in solely biofilm PN/A systems (Fux *et al.*,
403 2004, Gilbert *et al.*, 2015a, Isanta *et al.*, 2015, Lotti *et al.*, 2014, Park *et al.*, 2014, Poot *et al.*, 2016,
404 Veuillet *et al.*, 2014). Here, the actual nitrification activity of the NOB ($r_{\text{NOB,cycle}}$) in the biofilm was
405 consistently controlled by the DO, and was completely suppressed at $0.17 \text{ mg}_{\text{O}_2}\cdot\text{L}^{-1}$ (*Phase III* and *V*)
406 presumably due to diffusion limitations. To assess whether $r_{\text{NOB,cycle}}$ was suppressed only by DO
407 limitation or also by NO_2^- limitation, $r_{i,\text{cycle}}$ were measured under non-limiting NO_2^- concentrations.
408 No increase in $r_{\text{NOB,cycle}}$ was observed, confirming that DO rather than NO_2^- was the limiting
409 substrate for NOB in the biofilm (Figure 2c, vertical black arrows in *Phase V*). As a result of the
410 selective enrichment of AOB in the flocs, high NO_2^- fluxes to the biofilm for AMX can be
411 guaranteed at sufficiently low DO to suppress NOB activity in the biofilm.

412 **4.1.5 Effluent quality**

413 Overall, the wash-out of NOB from the flocs and the suppression of their activity in the biofilm at
414 low DO, resulted in N-removals over $88 \pm 4\%$ and a residual concentration of total N below 3
415 $\text{mg}_{\text{N}}\cdot\text{L}^{-1}$ ($1.9 \pm 0.5 \text{ mg}_{\text{NH}_4\text{-N}}\cdot\text{L}^{-1}$, $0.3 \pm 0.2 \text{ mg}_{\text{NO}_2\text{-N}}\cdot\text{L}^{-1}$, and $0.5 \pm 0.3 \text{ mg}_{\text{NO}_3\text{-N}}\cdot\text{L}^{-1}$). This is the highest
416 effluent quality reported so far for mainstream PN/A systems (De Clippeleir *et al.*, 2013, Gilbert *et*
417 *al.*, 2015a, Laurenzi *et al.*, 2016, Lotti *et al.*, 2014). Moreover, the aerobic N-removal rates achieved
418 ($79 \pm 16 \text{ mg}_{\text{N}}\cdot\text{L}^{-1}\cdot\text{d}^{-1}$), at an HRT of $11 \pm 2 \text{ h}$, were comparable to those of conventional WWTP

419 (Metcalf & Eddy *et al.*, 2013). The dynamics of influent and effluent concentrations are presented in
420 Figure S3.

421 **4.2 Mathematical modelling of the hybrid MBBR**

422 A simple dynamic model was developed to understand how the NOB concentration in the flocs
423 (X_{NOB}), respond to changes in DO, fraction of flocs removed per SBR cycle (f_{WAS}), and maximum
424 volumetric AMX activity in the biofilm ($r_{\text{AMX,max}}$). To assess the impact of the individual control
425 parameters four different scenarios were simulated (Table 3). The dynamics of X_{AOB} and X_{NOB} , and
426 effluent N concentrations are presented in Figure 4, and one cycle at pseudo steady-state is shown for
427 each scenario in Figure S5. The interdependences between the parameters and the impacts of
428 substrate affinities are also discussed.

429 **4.2.1 Scenario 1 (baseline): high AOB and NOB enrichment in the flocs**

430 A low initial concentration of $1 \text{ mg}_{\text{COD}}\cdot\text{L}^{-1}$ was set for X_{AOB} and X_{NOB} . Prolonged operation at 1.5
431 $\text{mg}_{\text{O}_2}\cdot\text{L}^{-1}$ resulted in the enrichment of both AOB and NOB in the flocs (Figure 4a), similar to
432 experimental observations during reactor operation (*Phase II*, Figure 2). The pseudo steady-state
433 X_{AOB} and X_{NOB} obtained in *Scenario 1* were assumed as initial concentrations for the other scenarios.

434 **4.2.2 Scenario 2: the DO controls the selective washout of NOB from the flocs**

435 The DO has a direct impact on the growth rate of both AOB and NOB (see process rates in Table 1).
436 AOB and NOB are also equally exposed to washout, *e.g.* by removing a fraction of flocs at the end
437 of each SBR cycle (f_{WAS}). However, only the NOB growth rate is impacted by the competition for
438 NO_2^- with the “ NO_2^- -sink” represented by the AMX in the biofilm. This direct competition for NO_2^-
439 between NOB and AMX leads to a difference in the actual growth rates of AOB and NOB (*i.e.*, μ_{NOB}
440 $< \mu_{\text{AOB}}$) providing the basis for the selective NOB washout (*i.e.*, $\mu_{\text{NOB}} < \text{SRT}^{-1} < \mu_{\text{AOB}}$).

441 The impact of a DO decrease to $0.15 \text{ mg}_{\text{O}_2}\cdot\text{L}^{-1}$ was assessed in *Scenario 2* to reflect the experimental
442 strategy (*Phase III*, Figure 2). Under the imposed DO-limiting condition, and at the fixed f_{WAS} , only

443 AOB could be maintained in the system while NOB were successfully washed out. High N-removals
444 are achieved (84%; Figures 4b, f). At the same time, due to the decreased AOB activity the HRT
445 increases from 1.6 to 5.9 h (*i.e.* longer cycles are required to achieve the set effluent NH_4^+
446 concentration). In terms of effluent concentrations, the reduction of the DO limits the aerobic activity
447 (as was the case in the reactor, Figure 2c) and results in the immediate reduction of NO_3^- (Figure 4f).
448 The numerical results provide a mechanistic interpretation for the experimental observations: the sole
449 reduction of the DO was sufficient to reduce the actual NOB growth rate below the minimum
450 required to prevent their washout. Moreover, the simulations support the possibility to use DO to
451 achieve the selective washout of NOB from the flocs.

452 **4.2.3 Scenario 3: increasing the fraction of flocs removed per cycle is an effective strategy to**
453 **achieve selective NOB washout**

454 Decreasing the DO might not always be a viable option at full scale, either because the operational
455 DO is already low or the size of the installed aerators and blowers is not suitable (Joss *et al.*, 2011).
456 Conversely, the selective removal of the flocs from a hybrid MBBR, or of fine particles from a
457 granular sludge system, may be a more feasible option, *e.g.*, via a separate settler (Veuillet *et al.*,
458 2014), hydrocyclone (Wett *et al.*, 2015), or screen (Han *et al.*, 2016). Simulations were run to assess
459 the effectiveness of increasing the fraction of flocs removed at the end of each SBR cycle as a
460 strategy to achieve the selective washout of NOB.

461 Numerical results suggest that successful NOB washout can indeed be achieved by increasing f_{WAS}
462 while maintaining all other conditions unchanged. Under *Scenario 3*, only the f_{WAS} was increased to
463 1.7 % and, as a result, NOB were selectively washed out at an SRT of 6.8 d (Figure 4c). In this case,
464 the actual NOB growth rate (function of DO and NO_2^- concentrations, Table 1) is no longer sufficient
465 to compensate for the increased washout. Simultaneously, the significantly lower AOB
466 concentrations maintained in the system result in higher HRT and thus reduced N-loads that can be
467 treated at the same effluent quality (Eq. 7). Nevertheless, in comparison to lowering the DO,

468 increasing f_{WAS} allows a faster NOB washout. From a process control perspective, the proposed
469 simulation examples highlight how in principle NOB can be washed out by only controlling the
470 removal of the flocs.

471 **4.2.4 Scenario 4: variations of AMX activity in the biofilm - the “NO₂-sink” - have a direct**
472 **impact on NOB concentration in the flocs**

473 The NOB in the flocs compete for NO₂⁻ with the AMX enriched in the biofilm - the “NO₂-sink” -
474 here represented by the maximum volumetric AMX activity ($r_{AMX,max}$). Increasing $r_{AMX,max}$, *i.e.* the
475 rate of NO₂⁻ consumption by AMX, reduces the bulk NO₂⁻ concentration and consequently the actual
476 NOB growth rate analogously to decreasing the DO.

477 The possibility of achieving complete and selective NOB washout from the flocs by increasing
478 $r_{AMX,max}$ was shown numerically. Under *Scenario 4*, the increase in $r_{AMX,max}$ resulted in a higher NO₂⁻
479 consumption, and thus a stronger competition with NOB, which are successfully washed out (Figure
480 4d). At the same time, simulations indicate that increasing $r_{AMX,max}$ results in slightly lower AOB
481 concentrations, as AMX reduce the NH₄⁺ available for AOB growth, with however minor
482 implications in terms of HRT. As a result, a high N-removal is achieved while still maintaining a low
483 HRT. The dynamics in effluent N concentrations are similar to *Scenario 2*. An immediate decrease of
484 the NO₃⁻ concentration, due to the reduced NO₂⁻ available for NOB, is followed by a further
485 progressive reduction as NOB are washed out (Figure 4h).

486 At full scale, the maximum AMX activity can in principle be increased, *e.g.* by bio-augmentation
487 from a sidestream PN/A process (Wett *et al.*, 2015). On the other hand, a partial or complete
488 inhibition of the AMX guild represents the opposite case where NOB may grow in the flocs due to
489 the reduced competition for NO₂⁻. Under such circumstances, increasing f_{WAS} and/or reducing the
490 DO may be suitable operational strategies to prevent NOB proliferation, as will be discussed in the
491 next section.

492 **4.2.5 Interdependent impacts of DO, f_{WAS} , and $r_{AMX,max}$, on NOB, and the impact of substrates**
493 **diffusion in the biofilm**

494 To better understand the interdependence between the different control parameters, the pseudo
495 steady-state concentrations of X_{AOB} , X_{NOB} and effluent NO_3^- are shown in Figure 5 as a function of
496 different $r_{AMX,max}$ and f_{WAS} . Two DO concentrations were simulated (0.15 and 1.5 $mg_{O_2} \cdot L^{-1}$),
497 representative of the low and high DO experimental periods. The pseudo steady-state of the four
498 scenarios discussed in the previous sections are highlighted.

499 X_{NOB} and the effluent NO_3^- concentration decrease with increasing $r_{AMX,max}$ (*i.e.* the competing
500 “ NO_2 -sink”). For any given DO and f_{WAS} , there is a minimum $r_{AMX,max}$ required for full NOB
501 washout from the flocs (Figures 5b, e). X_{AOB} also decrease with increasing $r_{AMX,max}$. In fact, by
502 consuming NH_4^+ , AMX reduce its availability for AOB growth (Figures 5a, d). This effect
503 disappears, and X_{AOB} stabilizes, as soon as the NOB are fully washed out. As a matter of fact, when
504 present in the system, NOB consume NO_2^- and indirectly favour AOB by decreasing NH_4^+ depletion
505 by AMX. As an example, the case of partial AMX inhibition would be equivalent to moving
506 horizontally to the left in Figure 5: an increased X_{NOB} is to be expected unless *e.g.* DO is decreased
507 or/and f_{WAS} is increased.

508 Additional simulations with a conservative ten-times higher value for both NH_4^+ and NO_2^- affinity
509 constants of AMX were run to assess the effects of substrate diffusion through the biofilm on the
510 modelled pseudo steady-states. Only the case of f_{WAS} equal to 0.5% was considered. As can be seen
511 from Figure 5, differences from the reference case (*i.e.* with unmodified affinity constants) are
512 negligible. It is therefore deemed justified to neglect diffusion effects for the purpose of this work.

513 Overall, when interpreting the numerical results, it is important to consider the simplifying
514 assumptions made in the modelling of the biofilm. AMX inhibition by oxygen was neglected, and the
515 $r_{AMX,max}$ was assumed to be the result of the active AMX in the anoxic layers of a deep biofilm. In
516 addition, no NOB growth in the biofilm was considered. In this respect, it is worth noting that the

517 nitrifying activity of NOB was shown experimentally to be completely suppressed at low DO.
518 Additional simulations with more complex models, including biomass stratification and inhibition
519 processes, are recommended here. Nevertheless, the simplified model allowed to identify the
520 fundamental role played by the AMX-enriched biofilm (“NO₂-sink”) in favouring the selective NOB
521 washout from the flocs.

522 **4.2.6 The possibility of successful NOB washout from the flocs is not impaired by the values of** 523 **the affinity constants**

524 In solely biofilm PN/A systems, the ratio of the oxygen affinity constants, $K_{O_2,NOB}/K_{O_2,AOB}$, and the
525 ratio of the NO₂⁻ affinity constants, $K_{NO_2,NOB}/K_{NO_2,AMX}$, are reported as the main parameters
526 controlling microbial competition (Brockmann and Morgenroth 2010, Hao *et al.*, 2002, Pérez *et al.*,
527 2014, Picioreanu *et al.*, 2016). For example, Hao *et al.*, (2002) have reported that $K_{O_2,NOB}/K_{O_2,AOB} >$
528 0.2 and $K_{NO_2,NOB}/K_{NO_2,AMX} > 3$ is a required condition for successful NOB suppression in a biofilm
529 system modelled at 30°C. In the present study, the sensitivity of the simulation results and the
530 validity of the previously drawn conclusions was tested with respect to the ratios $K_{O_2,NOB}/K_{O_2,AOB}$
531 and $K_{NO_2,NOB}/K_{NO_2,AMX}$. To ease the interpretation of the sensitivity analysis, $K_{O_2,AOB}$ was maintained
532 constant ($0.6 \text{ mg}_{O_2} \cdot L^{-1}$), and the $K_{O_2,NOB}/K_{O_2,AOB}$ ratio was varied between 0.14 (Regmi *et al.*, 2014)
533 and 2.00 (Perez *et al.*, 2014) by changing $K_{O_2,NOB}$ (Table S1). Simulations were run for the two
534 reference DO of 0.15 and $1.5 \text{ mg}_{O_2} \cdot L^{-1}$, and a fixed f_{WAS} of 0.5%. The pseudo steady-state X_{NOB} and
535 effluent NO₂⁻ concentrations are displayed as a function of $K_{O_2,NOB}/K_{O_2,AOB}$ in Figure 6. An overview
536 of X_{AOB} and X_{NOB} , and the effluent concentrations of the dissolved N species, is presented in Figure
537 S8.

538 At a low DO ($0.15 \text{ mg}_{O_2} \cdot L^{-1}$), the value of $K_{O_2,NOB}/K_{O_2,AOB}$ determines the mechanisms controlling
539 NOB washout. On the one hand, for values of $K_{O_2,NOB}/K_{O_2,AOB} < 1$, low NO₂⁻ concentrations are
540 modelled (*i.e.* rapidly consumed by NOB and AMX), and the competition with AMX for NO₂⁻ is the
541 dominant mechanism controlling NOB washout. Increasing $r_{AMX,max}$ results in lower NOB pseudo

542 steady-state concentrations (Figure 6a). Importantly, NOB are successfully washed out in the model
543 even in the extreme case of $K_{O_2,NOB}/K_{O_2,AOB} = 0.14$ (Regmi *et al.*, 2014), which would make their
544 control challenging in solely biofilm systems (Brockmann and Morgenroth 2010, Hao *et al.*, 2002,
545 Pérez *et al.*, 2014). On the other hand, for higher values ($K_{O_2,NOB}/K_{O_2,AOB} > 1$), DO limitation starts
546 to play an important role. Due to the reduced NOB growth rate, lower NOB concentrations can be
547 sustained in the system, and NO_2^- accumulates if the AMX activity is not sufficiently high (Figure
548 6b). Interestingly, for large $K_{O_2,NOB}$ ($K_{O_2,NOB}/K_{O_2,AOB} = 2.00$), NOB are washed out from the system
549 even in the absence of AMX and despite high NO_2^- accumulation. In this case, the actual NOB
550 growth rate is not sufficient to maintain them in the system at the cycle length set by AOB and the
551 imposed f_{WAS} (Eq. 7). Importantly, if $r_{AMX,max}$ is sufficiently high (*e.g.* $> 65 \text{ mg}_N \cdot \text{L}^{-1} \cdot \text{d}^{-1}$), the NOB
552 washout does not depend on $K_{O_2,NOB}/K_{O_2,AOB}$.

553 At a high DO ($1.5 \text{ mg}_{O_2} \cdot \text{L}^{-1}$), NOB washout is less sensitive to the value of $K_{O_2,NOB}/K_{O_2,AOB}$, and the
554 competition for NO_2^- with AMX is the dominant mechanism controlling NOB washout (Figure 6c).
555 Nevertheless, in analogy to the low DO case, NO_2^- accumulation occurs for high values of
556 $K_{O_2,NOB}/K_{O_2,AOB}$. Taken together, these results provide a mechanistic hypothesis to explain the
557 seemingly contradictory experimental observations during *Phase IV* (Figure 2), when only limited
558 NOB enrichment was observed in the flocs despite high DO and pronounced NO_2^- accumulation. In
559 general, higher $r_{AMX,max}$ are required for NOB washout (*e.g.*, $> 237 \text{ mg}_N \cdot \text{L}^{-1} \cdot \text{d}^{-1}$) compared to the case
560 at low DO.

561 In terms of NO_2^- affinity constants, $K_{NO_2,NOB}$ was decreased from a usually assumed value 100 times
562 higher than $K_{NO_2,AMX}$ (Hao *et al.*, 2002, Pérez *et al.*, 2014) to a value of $0.1 K_{NO_2,AMX}$ (Figure S9).
563 Decreasing $K_{NO_2,NOB}$ increases the competitive advantage of NOB over AMX and results in higher
564 X_{NOB} at pseudo steady-state for any given $r_{AMX,max}$. Nevertheless, within the broad range of values
565 tested, NOB washout can always be achieved provided that a sufficiently high $r_{AMX,max}$ is present
566 (Figure S9).

567 In summary, this work strongly support the increased operational flexibility offered by hybrid
568 systems, as compared to solely biofilm systems, for the control of NOB under mainstream
569 conditions. In fact, irrespective of the values chosen for the affinity constants, it is in principle
570 always possible to control the selective pressure on NOB via DO, f_{WAS} , and/or $r_{AMX,max}$, and achieve
571 their complete washout.

572

ACCEPTED MANUSCRIPT

573 **5 Conclusions**

574 This study aimed at understanding the mechanisms underlying microbial competition and the control
575 of NOB in hybrid PN/A reactors. To this end, a hybrid MBBR was operated under mainstream
576 conditions and a simple mathematical model of the system was developed. Experimentally, AMX
577 were shown to enrich in the biofilm while AOB and NOB grew preferentially in the flocs. AMX are
578 retained in the biofilm independent of floc removal and they act as a “NO₂-sink”. Conversely, AOB
579 and NOB are maintained in the flocs only if their actual growth rates is larger than the imposed
580 washout (*i.e.*, if $\mu > \text{SRT}^{-1}$).

- 581 • The key mechanisms for selectively washing out NOB from the system are maintaining a
582 sufficiently low SRT for the flocs and limiting NO₂⁻ bulk phase concentrations by means of
583 the AMX “NO₂-sink”. AOB growth rates are not affected by NO₂⁻ bulk phase concentrations
584 allowing reactor operation with selective washout of NOB while keeping AOB.
- 585 • Experimental results and numerical simulations showed that, for an imposed fraction of flocs
586 removed per SBR cycle or given SRT, NOB can be selectively washed out by decreasing the
587 DO-setpoint, *e.g.*, from 1.2 to 0.17 mg_{O₂}·L⁻¹. In this case, while both AOB and NOB actual
588 growth rates decrease; due to the concurrent NO₂-limitation only NOB growth rate is reduced
589 below the washout threshold *i.e.*, $\mu_{\text{NOB}} < \text{SRT}^{-1} < \mu_{\text{AOB}}$.
- 590 • In analogy, for a given DO-setpoint, simulations indicated that selective NOB washout can be
591 achieved also by increasing the fraction of flocs removed: the actual NOB growth rate
592 remains unaffected but is no longer sufficient to compensate for the increased washout.
- 593 • Moreover, differently from pure biofilm systems where NOB suppression relies on a larger
594 oxygen affinity of AOB than NOB, modelling results suggest that it is in principle always
595 possible to selectively wash out NOB by controlling the DO-setpoint and/or the flocs removal
596 provided AMX act as “NO₂-sink” in the biofilm.

597 Ultimately, this study demonstrates the high operational flexibility, in terms of variables that can be
598 easily controlled by operators, offered by hybrid systems for the control of NOB in mainstream
599 PN/A applications.

600

601

ACCEPTED MANUSCRIPT

6 Acknowledgements

602
603 This study was funded by the European Research Council ERC via the ATHENE project (grant
604 agreement 267897). ML was partially supported by a Marie Skłodowska-Curie Individual
605 Fellowship (MixAmox project; grant agreement 752992). We sincerely thank Kai Udert, Nicolas
606 Derlon and Fabrizio Sabba for valuable discussions, Marco Kipf for his support in the laboratory,
607 Brian Sinnet for the particle size analysis, and Claudia Baenninger-Werffeli, Sylvia Richter, and
608 Karin Rottermann for their assistance with the physicochemical analyses of all the samples.

ACCEPTED MANUSCRIPT

609 **7 References**

- 610 Anthonisen, A.C., Loehr, R.C., Prakasam, T.B. and Srinath, E.G. (1976) Inhibition of nitrification by
611 ammonia and nitrous acid. *Journal of the Water Pollution Control Federation* 48(5), 835-852.
- 612 APHA (2005) *Standard methods for the examination of water and wastewater*, Washington, D.C.
- 613 Brockmann, D. and Morgenroth, E. (2010) Evaluating operating conditions for outcompeting nitrite
614 oxidizers and maintaining partial nitrification in biofilm systems using biofilm modeling and
615 Monte Carlo filtering. *Water Research* 44(6), 1995-2009.
- 616 Corbala-Robles, L., Picioreanu, C., van Loosdrecht, M.C. and Perez, J. (2016) Analysing the effects
617 of the aeration pattern and residual ammonium concentration in a partial nitrification-anammox
618 process. *Environmental Technology* 37(6), 694-702.
- 619 De Clippeleir, H., Vlaeminck, S.E., De Wilde, F., Daeninck, K., Mosquera, M., Boeckx, P.,
620 Verstraete, W. and Boon, N. (2013) One-stage partial nitrification/anammox at 15°C on
621 pretreated sewage: feasibility demonstration at lab-scale. *Applied Microbiology and
622 Biotechnology* 97(23), 10199-10210.
- 623 Fux, C., Huang, D., Monti, A. and Siegrist, H. (2004) Difficulties in maintaining long-term partial
624 nitrification of ammonium-rich sludge digester liquids in a moving-bed biofilm reactor (MBBR).
625 *Water Science and Technology* 49(11-12), 53-60.
- 626 Gilbert, E.M., Agrawal, S., Schwartz, T., Horn, H. and Lackner, S. (2015a) Comparing different
627 Reactor Configurations for Partial Nitrification/Anammox at low Temperatures. *Water Research*.
- 628 Gilbert, E.M., Agrawal, S., Schwartz, T., Horn, H. and Lackner, S. (2015b) Comparing different
629 reactor configurations for Partial Nitrification/Anammox at low temperatures. *Water Research*
630 81, 92-100.
- 631 Han, M., Vlaeminck, S.E., Al-Omari, A., Wett, B., Bott, C., Murthy, S. and De Clippeleir, H. (2016)
632 Uncoupling the solids retention times of flocs and granules in mainstream deammonification:
633 A screen as effective out-selection tool for nitrite oxidizing bacteria. *Bioresource Technology*
634 221, 195-204.
- 635 Hao, X., Heijnen, J.J. and van Loosdrecht, M.C.M. (2002) Sensitivity analysis of a biofilm model
636 describing a one-stage completely autotrophic nitrogen removal (CANON) process.
637 *Biotechnology and Bioengineering* 77(3), 266-277.
- 638 Hellinga, C., Schellen, A.A.J.C., Mulder, J.W., van Loosdrecht, M.C.M. and Heijnen, J.J. (1998) The
639 SHARON process: an innovative method for nitrogen removal from ammonium-rich waste
640 water. *Water Science and Technology* 37(9), 135-142.
- 641 Hubaux, N., Wells, G. and Morgenroth, E. (2015) Impact of coexistence of flocs and biofilm on
642 performance of combined nitrification-anammox granular sludge reactors. *Water Research* 68,
643 127-139.
- 644 Isanta, E., Reino, C., Carrera, J. and Perez, J. (2015) Stable partial nitrification for low-strength
645 wastewater at low temperature in an aerobic granular reactor. *Water Research* 80, 149-158.
- 646 Joss, A., Derlon, N., Cyprien, C., Burger, S., Szivák, I., Traber, J., Siegrist, H. and Morgenroth, E.
647 (2011) Combined nitrification-anammox: advances in understanding process stability.
648 *Environmental Science & Technology* 45(22), 9735-9742.
- 649 Jubany, I., Lafuente, J., Baeza, J.A. and Carrera, J. (2009) Total and stable washout of nitrite
650 oxidizing bacteria from a nitrifying continuous activated sludge system using automatic control
651 based on Oxygen Uptake Rate measurements. *Water Research* 43(11), 2761-2772.
- 652 Lackner, S., Gilbert, E.M., Vlaeminck, S.E., Joss, A., Horn, H. and van Loosdrecht, M.C.M. (2014)
653 Full-scale partial nitrification/anammox experiences - An application survey. *Water Research* 55,
654 292-303.
- 655 Laurenzi, M., Falås, P., Robin, O., Wick, A., Weissbrodt, D.G., Nielsen, J.L., Ternes, T.A.,
656 Morgenroth, E. and Joss, A. (2016) Mainstream partial nitrification and anammox: long-term
657 process stability and effluent quality at low temperatures. *Water Research* 101, 628-639.

- 658 Lauren, M., Weissbrodt, D.G., Szivak, I., Robin, O., Nielsen, J.L., Morgenroth, E. and Joss, A.
659 (2015) Activity and growth of anammox biomass on aerobically pre-treated municipal
660 wastewater. *Water Research* 80, 325-336.
- 661 Leix, C., Drewes, J.E. and Koch, K. (2016) The role of residual quantities of suspended sludge on
662 nitrogen removal efficiency in a deammonifying moving bed biofilm reactor. *Bioresource*
663 *Technology* 219, 212-218.
- 664 Liu, G. and Wang, J. (2013) Long-term low DO enriches and shifts nitrifier community in activated
665 sludge. *Environmental Science & Technology* 47(10), 5109-5117.
- 666 Lotti, T., Kleerebezem, R., Hu, Z., Kartal, B., de Kreuk, M., van Erp Taalman Kip, C., Kruit, J.,
667 Hendrickx, T.L.G. and van Loosdrecht, M.C.M. (2015) Pilot-scale evaluation of anammox-
668 based mainstream nitrogen removal from municipal wastewater. *Environmental Technology*
669 36(9), 1167-1177.
- 670 Lotti, T., Kleerebezem, R., Hu, Z., Kartal, B., Jetten, M.S.M. and van Loosdrecht, M.C.M. (2014)
671 Simultaneous partial nitrification and anammox at low temperature with granular sludge. *Water*
672 *Research* 66, 111-121.
- 673 Malovanyy, A., Trela, J. and Plaza, E. (2015) Mainstream wastewater treatment in integrated fixed
674 film activated sludge (IFAS) reactor by partial nitrification/anammox process. *Bioresource*
675 *Technology* 198, 478-487.
- 676 Metcalf & Eddy, I., Tchobanoglous, G., Stensel, H.D., Tsuchihashi, R. and Burton, F. (2013)
677 *Wastewater engineering: treatment and resource recovery*, McGraw-Hill Education.
- 678 Morgenroth, E. (2008) *Biological Wastewater Treatment - Principles, Modelling, and Design*. Henze,
679 M., van Loosdrecht, M.C.M., Ekama, G. and Brdjanovic, D. (eds), IWA Publishing, London.
- 680 Park, H., Sundar, S., Ma, Y. and Chandran, K. (2014) Differentiation in the microbial ecology and
681 activity of suspended and attached bacteria in a nitrification-anammox process. *Biotechnology*
682 *and Bioengineering* 112(2), 272-279.
- 683 Perez, J., Lotti, T., Kleerebezem, R., Picioreanu, C. and van Loosdrecht, M.C. (2014) Outcompeting
684 nitrite-oxidizing bacteria in single-stage nitrogen removal in sewage treatment plants: a model-
685 based study. *Water Research* 66, 208-218.
- 686 Pérez, J., Lotti, T., Kleerebezem, R., Picioreanu, C. and van Loosdrecht, M.C.M. (2014)
687 Outcompeting nitrite-oxidizing bacteria in single-stage nitrogen removal in sewage treatment
688 plants: a model-based study. *Water Research*.
- 689 Picioreanu, C., Pérez, J. and van Loosdrecht, M.C.M. (2016) Impact of cell cluster size on apparent
690 half-saturation coefficients for oxygen in nitrifying sludge and biofilms. *Water Research* 106,
691 371-382.
- 692 Poot, V., Hoekstra, M., Geleijnse, M.A., van Loosdrecht, M.C. and Perez, J. (2016) Effects of the
693 residual ammonium concentration on NOB repression during partial nitrification with granular
694 sludge. *Water Research* 106, 518-530.
- 695 Regmi, P., Miller, M.W., Holgate, B., Bunce, R., Park, H., Chandran, K., Wett, B., Murthy, S. and
696 Bott, C.B. (2014) Control of aeration, aerobic SRT and COD input for mainstream
697 nitrification/denitrification. *Water Research* 57, 162-171.
- 698 Rittmann, B.E. and McCarty, P.L. (2001) *Environmental biotechnology: principles and applications*,
699 McGraw-Hill Education.
- 700 Shi, Y., Wells, G. and Morgenroth, E. (2016) Microbial activity balance in size fractionated
701 suspended growth biomass from full-scale sidestream combined nitrification-anammox reactors.
702 *Bioresource Technology* 218, 38-45.
- 703 Siegrist, H., Salzgeber, D., Eugster, J. and Joss, A. (2008) Anammox brings WWTP closer to energy
704 autarky due to increased biogas production and reduced aeration energy for N-removal. *Water*
705 *Science and Technology* 57(3), 383-388.
- 706 Sliekers, A.O., Haaijer, S.C., Stafsnes, M.H., Kuenen, J.G. and Jetten, M.S. (2005) Competition and
707 coexistence of aerobic ammonium- and nitrite-oxidizing bacteria at low oxygen concentrations.
708 *Applied Microbiology and Biotechnology* 68(6), 808-817.

- 709 Speth, D.R., In 't Zandt, M.H., Guerrero-Cruz, S., Dutilh, B.E. and Jetten, M.S. (2016) Genome-
710 based microbial ecology of anammox granules in a full-scale wastewater treatment system.
711 *Nature Communications* 7, 11172.
- 712 Takács, I., Stricker, A.-E., Achleitner, S., Barrie, A., Rauch, W. and Murthy, S. (2008) Do You
713 Know Your Sludge Age? *Proceedings of the Water Environment Federation* 2008(13), 3639-
714 3655.
- 715 van Loosdrecht, M.C.M. and Brdjanovic, D. (2014) Water treatment. Anticipating the next century
716 of wastewater treatment. *Science* 344(6191), 1452-1453.
- 717 Veuillet, F., Lacroix, S., Bausseron, A., Gonidec, E., Ochoa, J., Christensson, M. and Lemaire, R.
718 (2014) Integrated fixed-film activated sludge ANITAMox process - a new perspective for
719 advanced nitrogen removal. *Water Science and Technology* 69(5), 915-922.
- 720 Vlaeminck, S.E., Terada, A., Smets, B.F., De Clippeleir, H., Schaubroeck, T., Bolca, S., Demeestere,
721 L., Mast, J., Boon, N., Carballa, M. and Verstraete, W. (2010) Aggregate size and architecture
722 determine microbial activity balance for one-stage partial nitrification and anammox. *Applied
723 and Environmental Microbiology* 76(3), 900-909.
- 724 Volcke, E.I., Picioreanu, C., De Baets, B. and van Loosdrecht, M.C. (2012) The granule size
725 distribution in an anammox-based granular sludge reactor affects the conversion--implications
726 for modeling. *Biotechnology and Bioengineering* 109(7), 1629-1636.
- 727 Wells, G.F., Shi, Y., Laurenzi, M., Rosenthal, A., Szivak, I., Weissbrodt, D.G., Joss, A., Buerghmann,
728 H., Johnson, D.R. and Morgenroth, E. (2017) Comparing the Resistance, Resilience, and
729 Stability of Replicate Moving Bed Biofilm and Suspended Growth Combined Nitrification-
730 Anammox Reactors. *Environmental Science & Technology* 51(9), 5108-5117.
- 731 Wett, B., Podmirseg, S.M., Gómez-Brandón, M., Hell, M., Nyhuis, G., Bott, C. and Murthy, S.
732 (2015) Expanding DEMON Sidestream Deammonification Technology Towards Mainstream
733 Application. *Water Environment Research* 87(12), 2084-2089.
- 734 Winkler, M.K.H., Kleerebezem, R., Kuenen, J.G., Yang, J. and van Loosdrecht, M.C.M. (2011)
735 Segregation of Biomass in Cyclic Anaerobic/Aerobic Granular Sludge Allows the Enrichment
736 of Anaerobic Ammonium Oxidizing Bacteria at Low Temperatures. *Environmental Science &
737 Technology* 45(17), 7330-7337.
- 738 WPO (1998) Water Protection Ordinance of 28 October 1998 (814.201), UNECE, Geneva.

739

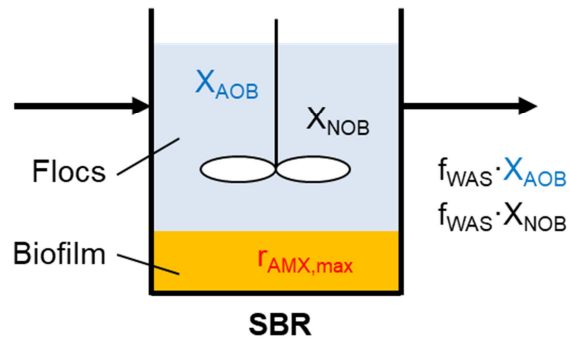


Figure 1: Location of the active biomass in the mathematical model of the hybrid system. The model assumes perfect biomass segregation, with AOB and NOB in the flocs and AMX in the biofilm. $r_{AMX,max}$ is the maximum volumetric anammox activity ($\text{mg}_{(\text{NH}_4+\text{NO}_2)\text{-N}}\cdot\text{L}^{-1}\cdot\text{d}^{-1}$). f_{WAS} represents the fraction of flocs removed at the end of each SBR cycle.

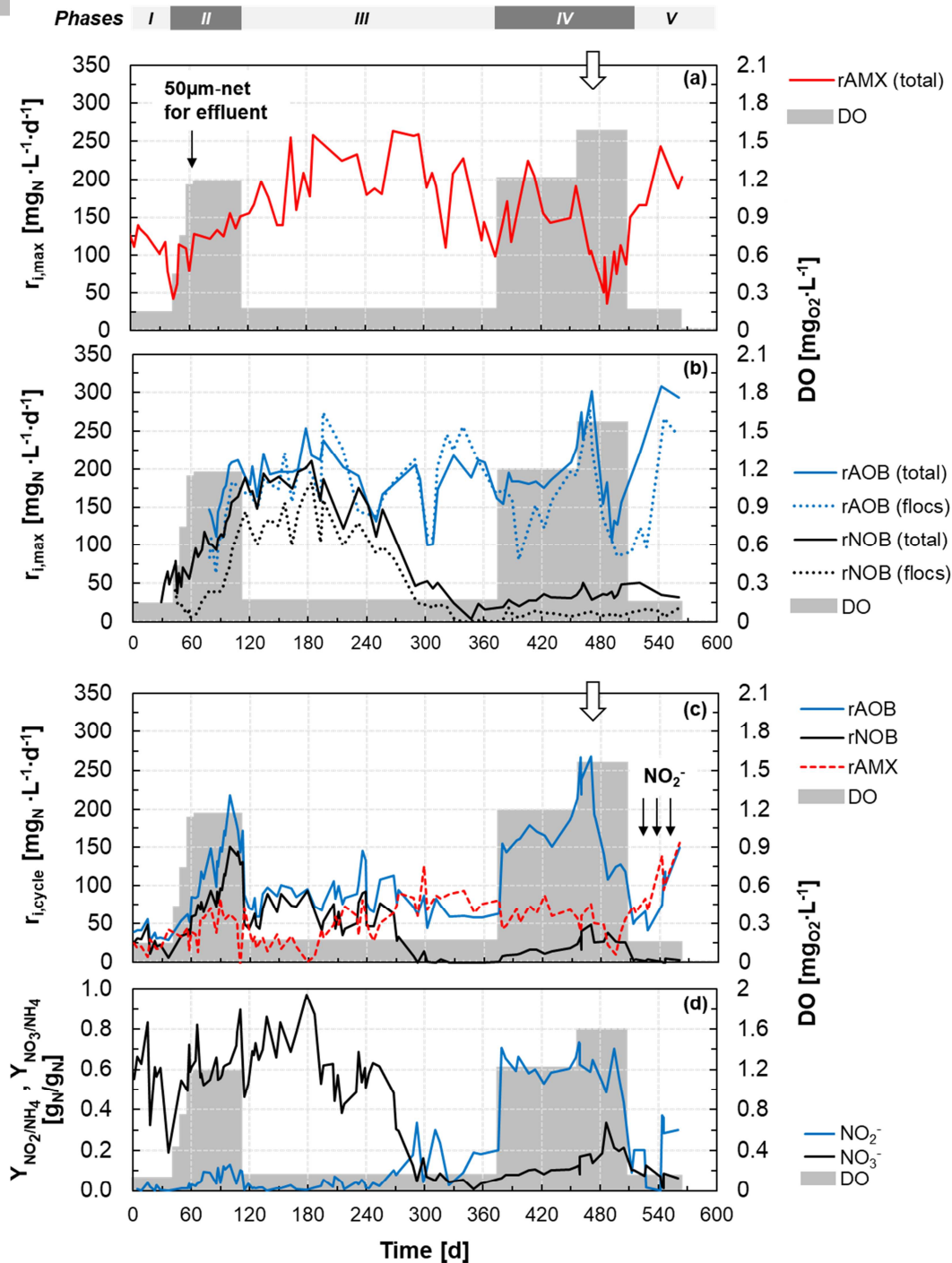


Figure 2: Time series of the maximum ($r_{i,max}$) and actual ($r_{i,cycle}$) volumetric activities of AOB, NOB, and AMX in the hybrid MBBR. (a) Total maximum volumetric activities of AMX (the activity in the flocs was negligible throughout the experimental period). (b) Segregation of maximum volumetric activities of AOB and NOB: total biomass (biofilm and flocs) and floc fraction only. (c) Actual volumetric activities measured during the aerobic phase of an SBR cycle. Activities are expressed as follows: AOB, mg_{NH₄-N}·L⁻¹·d⁻¹; NOB, mg_{NO₃-N}·L⁻¹·d⁻¹; AMX, mg_{(NH₄+NO₂)-N}·L⁻¹·d⁻¹. (d) Yields of NO₂⁻ and NO₃⁻ accumulated relative to the NH₄⁺ consumed during the aerobic phase. Shaded area: the average of the DO concentration measured during aeration over the representative periods. Vertical black arrows: in (a) time when floc retention was improved by filtering the effluent through a 50-µm-mesh sock-net; in (c) time when the volumetric activities during regular operation were measured under non-limiting nitrite concentrations. Vertical empty arrows: in (a, c) time of the prolonged rain event.

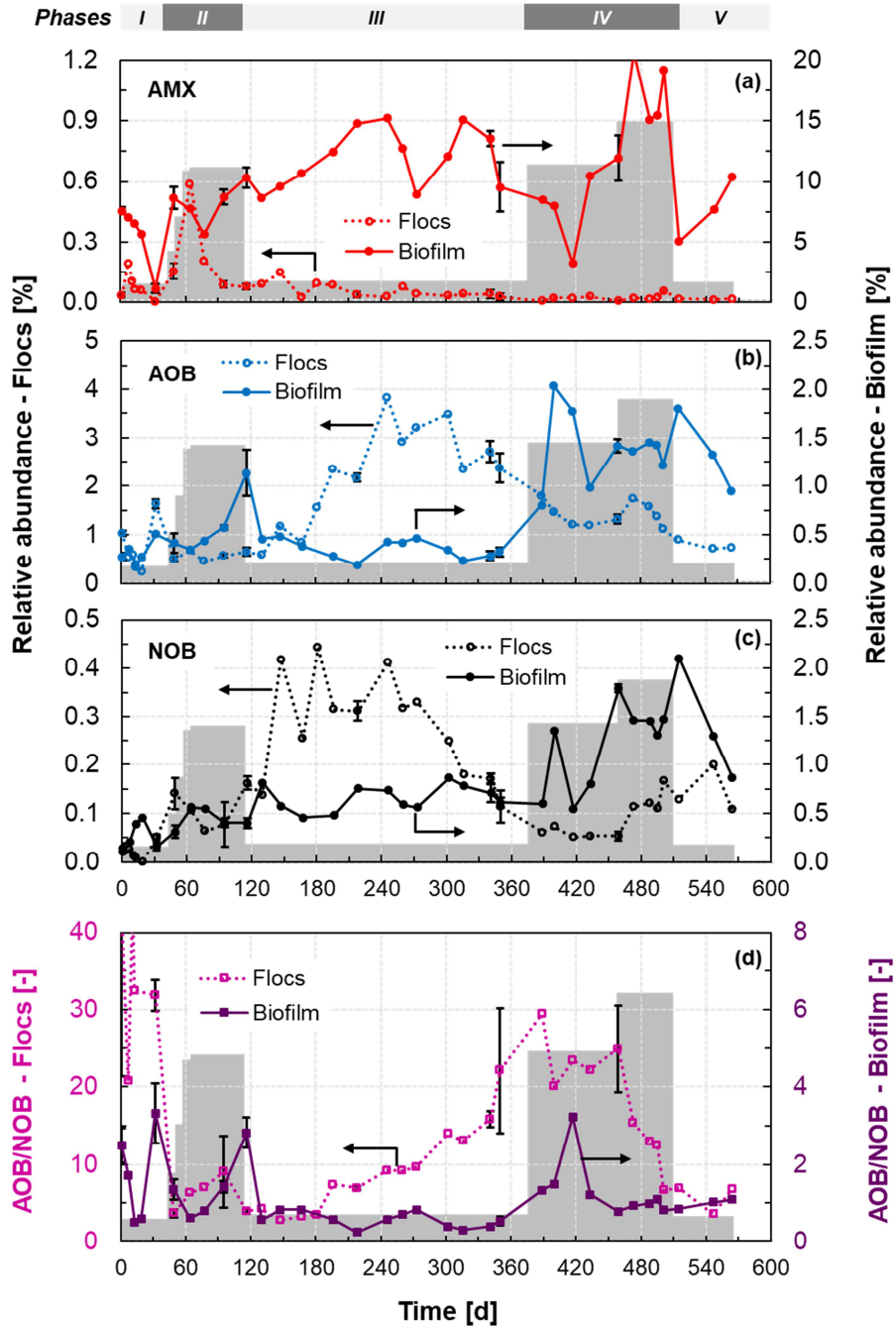


Figure 3: Time series of the relative abundances of AMX (a), AOB (b), and NOB (c) in the flocs (left y-axis) and biofilm (right y-axis) as estimated by 16S rRNA gene-based amplicon sequencing analysis. The displayed values represent the sum of the relative abundances of all OTUs detected for each guild. For the time series of the single OTUs, see Figure S4. (d) Time series of the dimensionless ratio between the relative abundance of AOB and the relative abundance of NOB in the flocs ($AOB/NOB - Flocs$) and biofilm ($AOB/NOB - Biofilm$). Shaded area: average operational DO concentration over the representative periods (for values, see Figure 2). Error bars: standard deviation of biological triplicates.

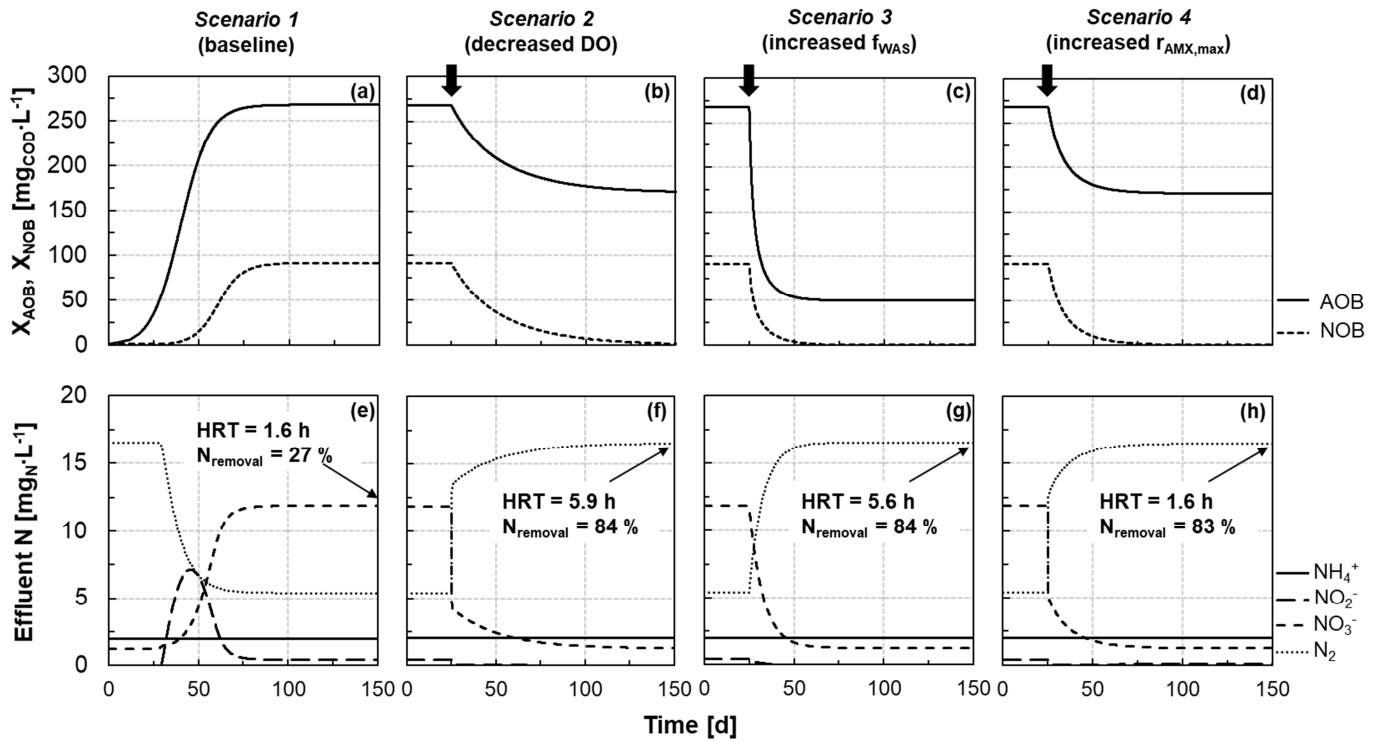


Figure 4: Results from mathematical modelling of dynamics in concentrations of AOB (X_{AOB}), NOB (X_{NOB}), and effluent N towards the pseudo steady-state for the four scenarios detailed in Table 3. Pseudo steady-state in *Scenario 1* is used as initial conditions for Scenarios 2, 3, and 4. Profiles of nitrogen species and biomass evolution during an SBR cycle at pseudo steady-state for the four scenarios are presented in Figure S6. Vertical thick arrows: times when scenario-specific modification of operational conditions was implemented.

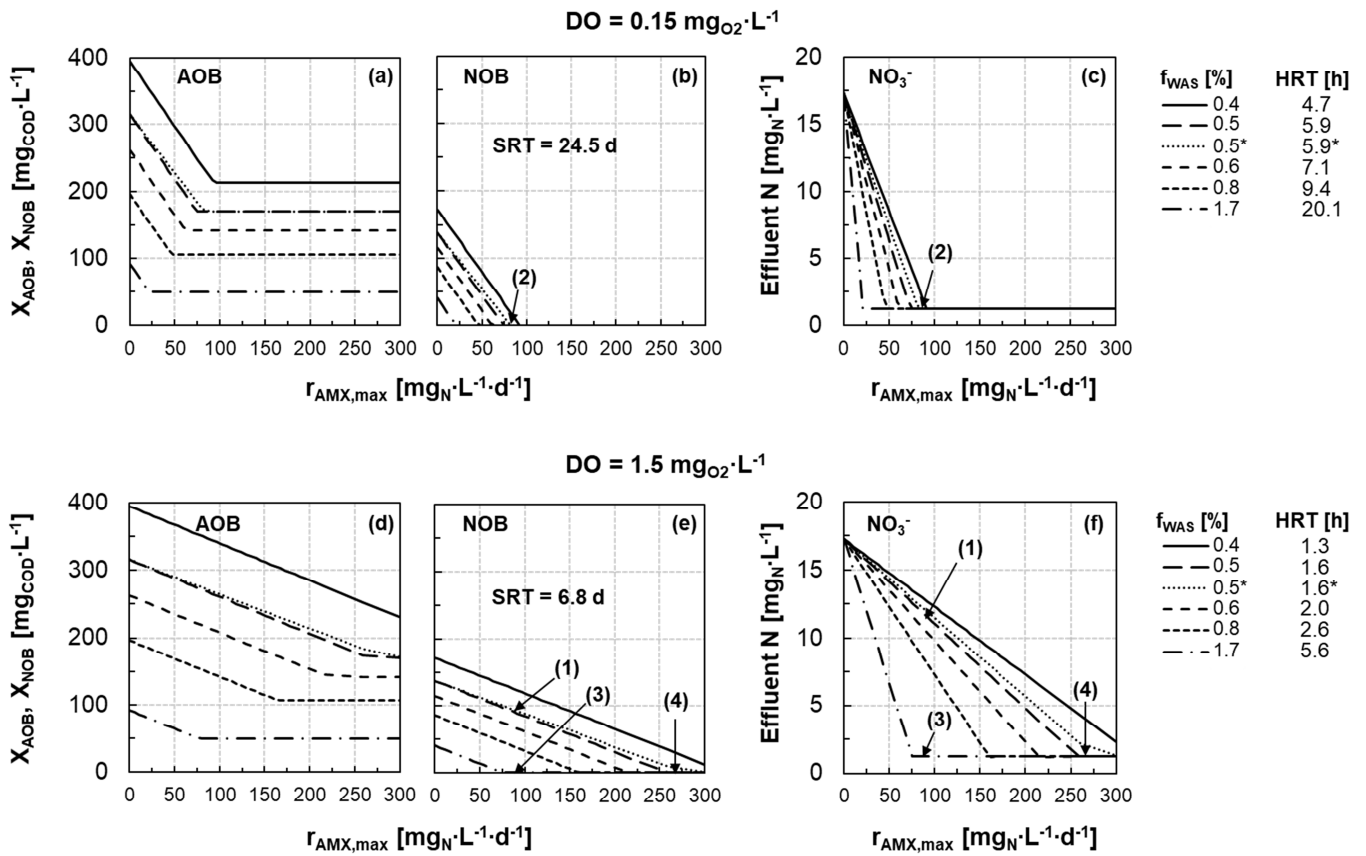


Figure 5: Concentrations of AOB (a, d) and NOB (b, e) in the flocs under pseudo steady-state conditions modelled as a function of the maximum volumetric AMX activity ($r_{AMX,max}$ mg_{(NH₄+NO₂)-N}·L⁻¹·d⁻¹) for two reference DO, 0.15 and 1.5 mg_{O2}·L⁻¹. (c, f) Residual concentration of NO₃⁻ in the effluent at pseudo steady-state. NH₄⁺, NO₂⁻ and N₂ concentrations are presented in Figure S5. The different lines represent different f_{WAS} values, as shown in the legend to the right of the figures. The resulting HRT for each f_{WAS} is also reported in the legend. Simulations were run with reference parameters shown in Table 2. Only for the case marked with (*), the ammonium and nitrite affinity constants of AMX were increased by a factor of ten. *Black arrows and numbers in parentheses:* the four scenarios discussed in the text and presented in Figure 4.

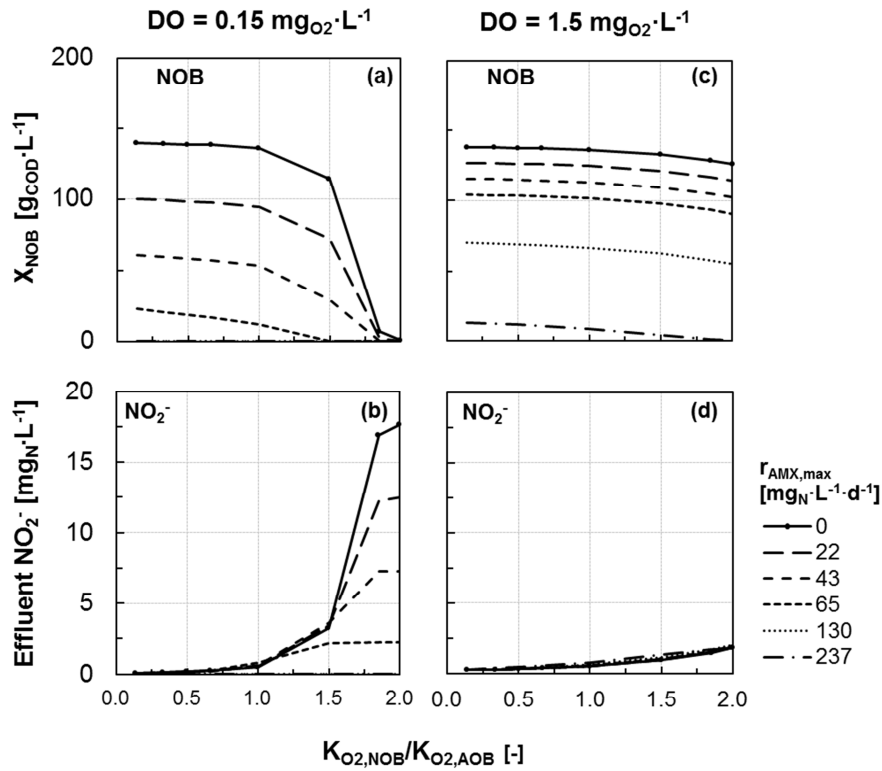


Figure 6: Sensitivity analysis. Impact of different $K_{\text{O}_2,\text{NOB}}/K_{\text{O}_2,\text{AOB}}$ on simulated NOB concentrations at pseudo steady-state (a, c) and corresponding effluent NO_2^- concentrations (b, d) for the two reference DO (0.15 and $1.5 \text{ mg}_{\text{O}_2}\cdot\text{L}^{-1}$). $K_{\text{O}_2,\text{NOB}}/K_{\text{O}_2,\text{AOB}} = 0.67$ is the reference case (see Table 2). The values of the oxygen affinities for NOB and AOB and their ratio are presented in Table S1. In the simulations, an f_{WAS} of 0.5% was assumed. All concentrations of X_{AOB} and effluent N species at pseudo steady-state are presented in Figure S8. $r_{\text{AMX,max}}$ is expressed as $\text{mg}_{(\text{NH}_4+\text{NO}_2)\text{-N}}\cdot\text{L}^{-1}\cdot\text{d}^{-1}$.

Table 1: Stoichiometric and kinetic matrix describing the growth of aerobic ammonium-oxidizing bacteria (AOB) and aerobic nitrite-oxidizing bacteria (NOB), and anaerobic ammonium-oxidizing bacteria (anammox, AMX). The matrix was used to estimate the activity of the three guilds during regular SBR operation ($r_{i,cycle}$), and for the dynamic model of the hybrid system (Figure 1). In the dynamic model, the maximum anammox process rate ($\rho_{AMX,max} = \mu_{AMX,max} \cdot X_{AMX}$) was assumed constant during each simulation. To this end, the concentration of AMX (X_{AMX}) was considered as a constant and not as a state variable, and is therefore omitted from the matrix.

Component	S_{O_2} $g_{O_2} \cdot m^{-3}$	S_{NH_4} $g_N \cdot m^{-3}$	S_{NO_2} $g_N \cdot m^{-3}$	S_{NO_3} $g_N \cdot m^{-3}$	S_{N_2} $g_N \cdot m^{-3}$	X_{AOB} $g_{COD} \cdot m^{-3}$	X_{NOB} $g_{COD} \cdot m^{-3}$	Process rates (ρ) $g_{COD} \cdot m^{-3} \cdot d^{-1}$
Processes								
AOB growth	$-\frac{(3.43 - Y_{AOB})}{Y_{AOB}}$	$-\frac{1}{Y_{AOB}} - i_{N,AOB}$	$\frac{1}{Y_{AOB}}$			1		$\mu_{AOB,max} \cdot X_{AOB} \cdot \frac{S_{NH_4}}{S_{NH_4} + K_{AOB,NH_4}} \cdot \frac{S_{O_2}}{S_{O_2} + K_{AOB,O_2}}$
NOB growth	$-\frac{(1.14 - Y_{NOB})}{Y_{NOB}}$	$-i_{N,NOB}$	$\frac{1}{Y_{NOB}}$	$\frac{1}{Y_{NOB}}$			1	$\mu_{NOB,max} \cdot X_{NOB} \cdot \frac{S_{NO_2}}{S_{NO_2} + K_{NOB,NO_2}} \cdot \frac{S_{O_2}}{S_{O_2} + K_{NOB,O_2}}$
AMX growth		$-\frac{1}{Y_{AMX}} - i_{N,AMX}$	$-\frac{1}{Y_{AMX}} - \frac{1}{1.14}$	$\frac{1}{1.14}$	$\frac{2}{Y_{AMX}}$			$\rho_{AMX,max} \cdot \frac{S_{NH_4}}{S_{NH_4} + K_{AMX,NH_4}} \cdot \frac{S_{NO_2}}{S_{NO_2} + K_{AMX,NO_2}}$
Composition Matrix								
gTOD	-1		-3.43	-4.57	-1.71	1	1	
gN		1	1	1	1	$i_{N,AOB}$	$i_{N,NOB}$	

Table 2: Kinetic and stoichiometric parameters.

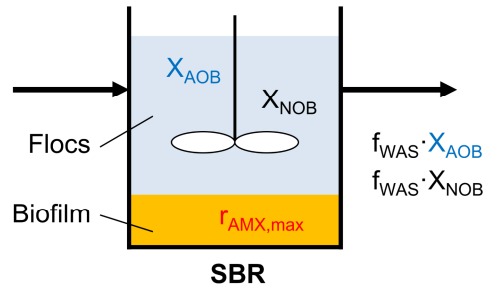
Aerobic ammonium-oxidizing bacteria (AOB)				
$\mu_{\text{AOB,max}}$	d^{-1}	Maximum specific growth rate	0.30	<i>This study*</i>
Y_{AOB}	$\text{g}_{\text{COD}} \cdot \text{g}_{\text{N}}^{-1}$	Growth yield	0.18	(Jubany <i>et al.</i> , 2009)
$K_{\text{NH}_4,\text{AOB}}$	$\text{g}_{\text{NH}_4\text{-N}} \cdot \text{m}^{-3}$	Ammonium half-saturation constant	2.4	(Wiesmann, 1994)
$K_{\text{O}_2,\text{AOB}}$	$\text{g}_{\text{COD}} \cdot \text{m}^{-3}$	Oxygen half-saturation constant	0.6	(Wiesmann, 1994)
$i_{\text{N,AOB}}$	$\text{g}_{\text{N}} \cdot \text{g}_{\text{COD}}^{-1}$	Nitrogen content in AOB	0.083	(Volcke <i>et al.</i> , 2010)
Aerobic nitrite-oxidizing bacteria (NOB)				
$\mu_{\text{NOB,max}}$	d^{-1}	Maximum specific growth rate	0.34	<i>This study*</i>
Y_{NOB}	$\text{g}_{\text{COD}} \cdot \text{g}_{\text{N}}^{-1}$	Growth yield	0.08	(Jubany <i>et al.</i> , 2009)
$K_{\text{O}_2,\text{NOB}}$	$\text{g}_{\text{COD}} \cdot \text{m}^{-3}$	Oxygen half-saturation constant	0.4	(Blackburne <i>et al.</i> , 2007)
$K_{\text{NO}_2,\text{NOB}}$	$\text{g}_{\text{NO}_2\text{-N}} \cdot \text{m}^{-3}$	Nitrite half-saturation constant	0.5	(Wiesmann, 1994)
$i_{\text{N,NOB}}$	$\text{g}_{\text{N}} \cdot \text{g}_{\text{COD}}^{-1}$	Nitrogen content in NOB	0.083	(Volcke <i>et al.</i> , 2010)
Anaerobic ammonium-oxidizing bacteria (AMX)				
$\rho_{\text{AMX,max}}$	$\text{mg}_{\text{COD}} \cdot \text{L}^{-1} \cdot \text{d}^{-1}$	Maximum AMX process rate	0 - 24	Assumed**
Y_{AMX}	$\text{g}_{\text{COD}} \cdot \text{g}_{\text{N}}^{-1}$	Growth yield	0.17	(Strous <i>et al.</i> , 1998)
$K_{\text{NH}_4,\text{AMX}}$	$\text{g}_{\text{NH}_4\text{-N}} \cdot \text{m}^{-3}$	Ammonium half saturation constant	0.03	(Volcke <i>et al.</i> , 2010)
$K_{\text{NO}_2,\text{AMX}}$	$\text{g}_{\text{NO}_2\text{-N}} \cdot \text{m}^{-3}$	Nitrite half saturation constant	0.005	(Volcke <i>et al.</i> , 2010)
$i_{\text{N,AMX}}$	$\text{g}_{\text{N}} \cdot \text{g}_{\text{COD}}^{-1}$	Nitrogen content in AMX	0.058	(Volcke <i>et al.</i> , 2010)

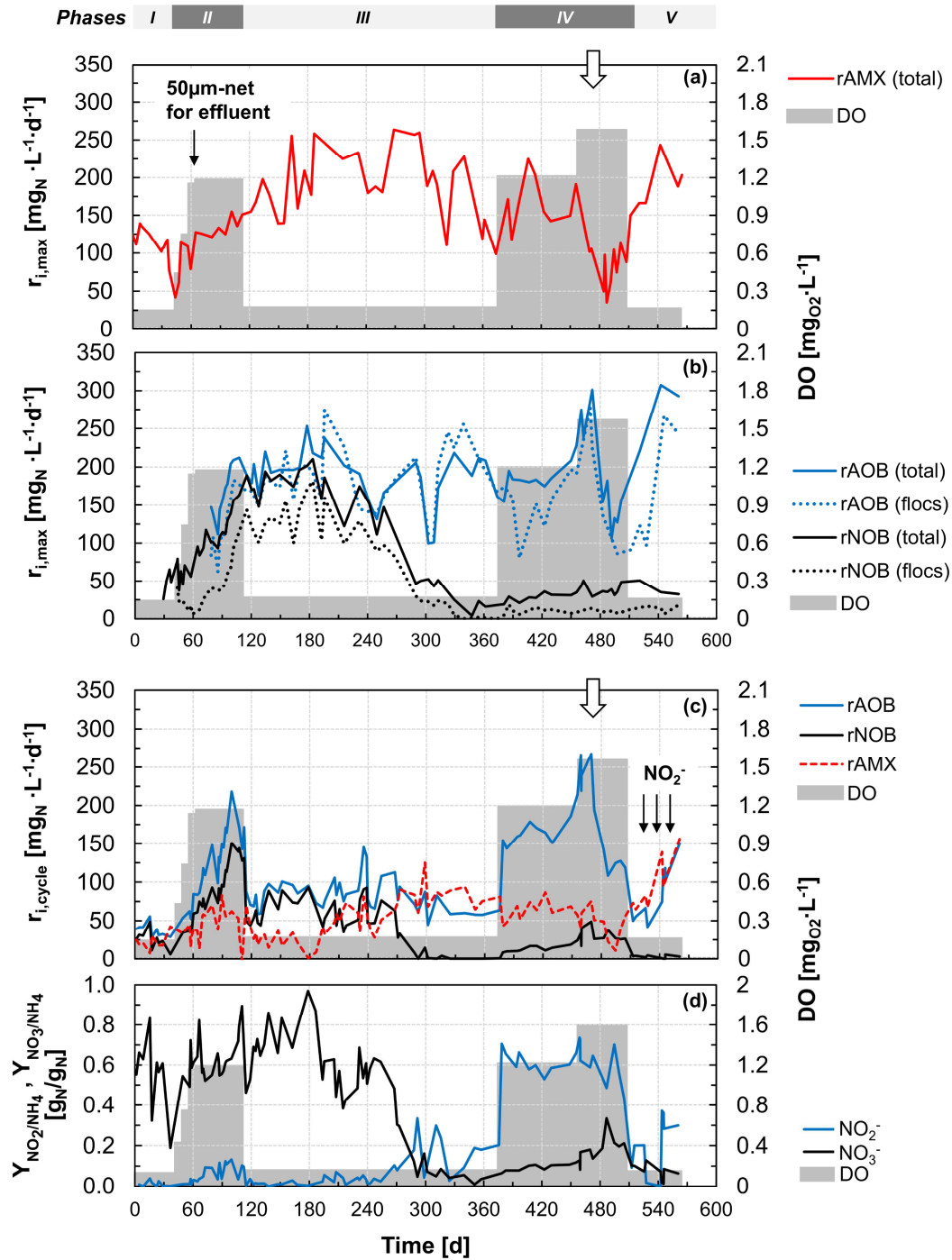
*Estimated from the maximum activity increase at 15°C during *Phase II* (Figure 2a).

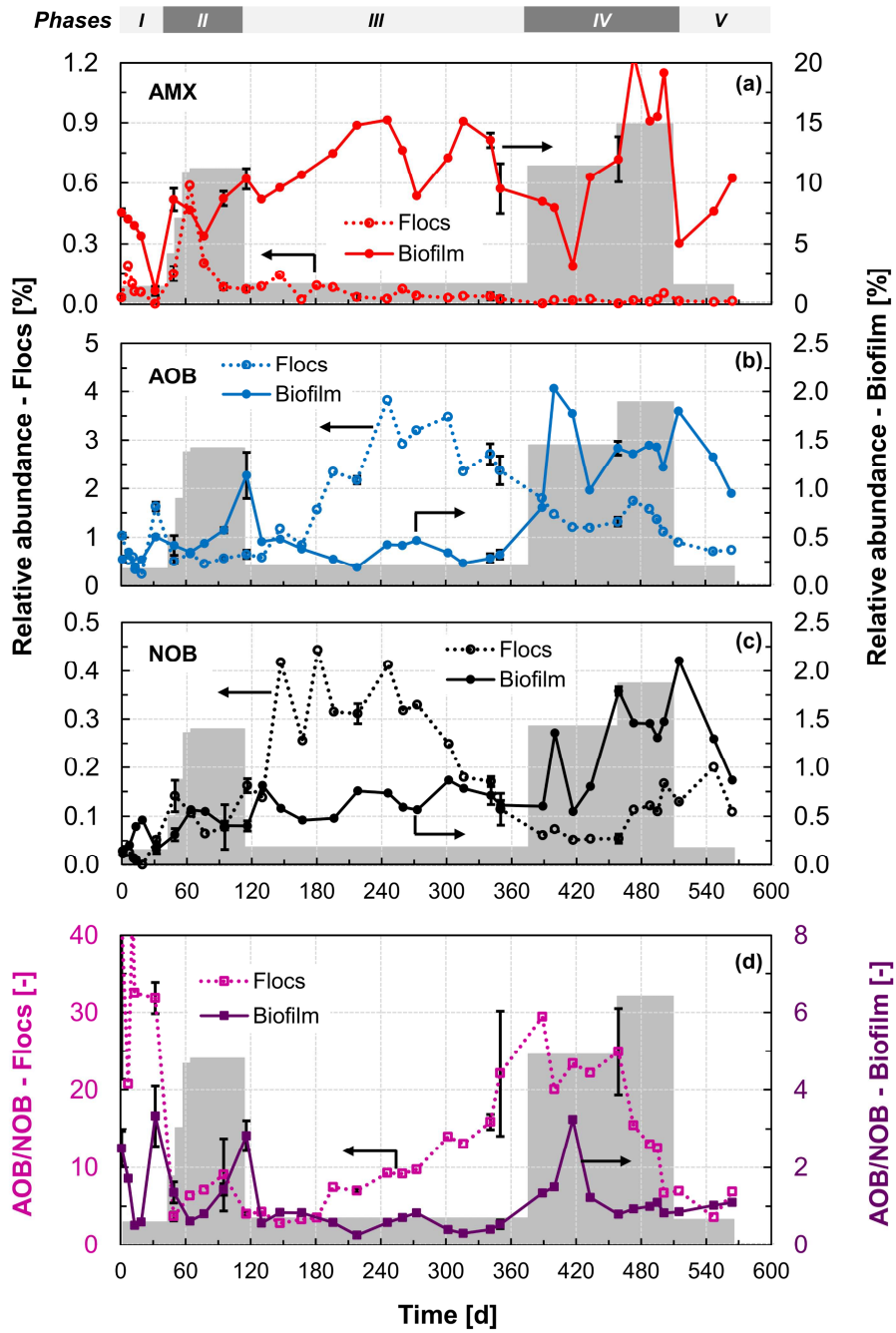
** Corresponding to $r_{\text{AMX,max}}$ in the range observed experimentally at 15°C, 0-300 $\text{mg}_{(\text{NH}_4+\text{NO}_2)\text{-N}} \cdot \text{L}^{-1} \cdot \text{d}^{-1}$

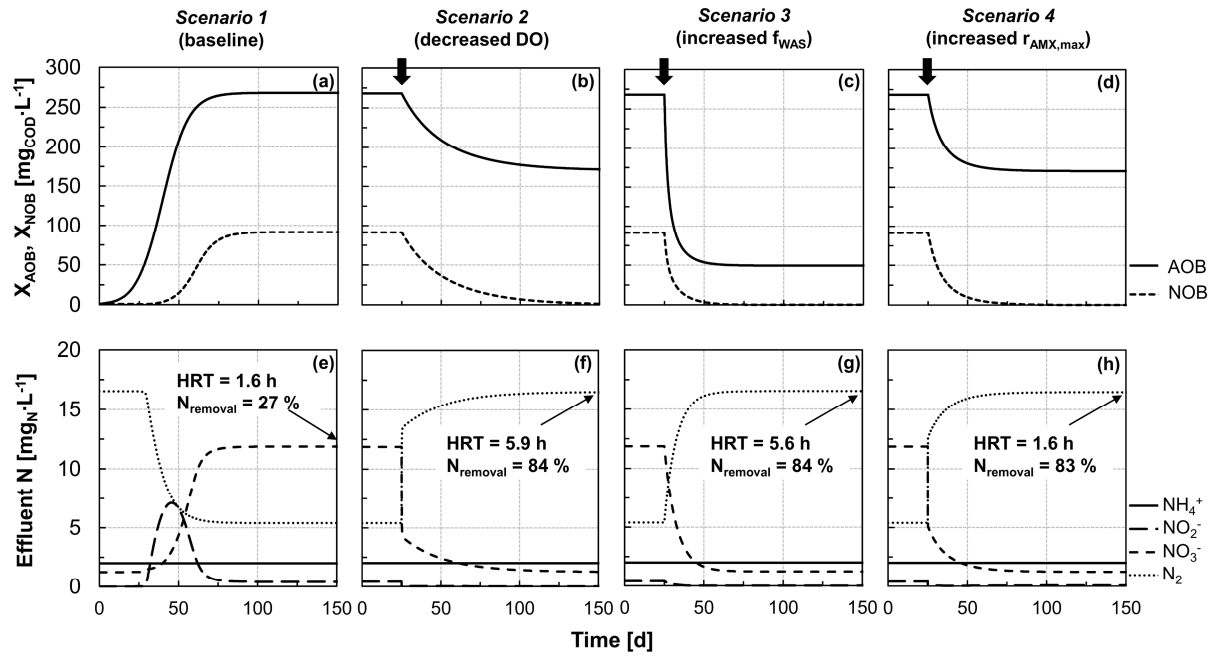
Table 3: Values of the control parameters for the four tested scenarios.

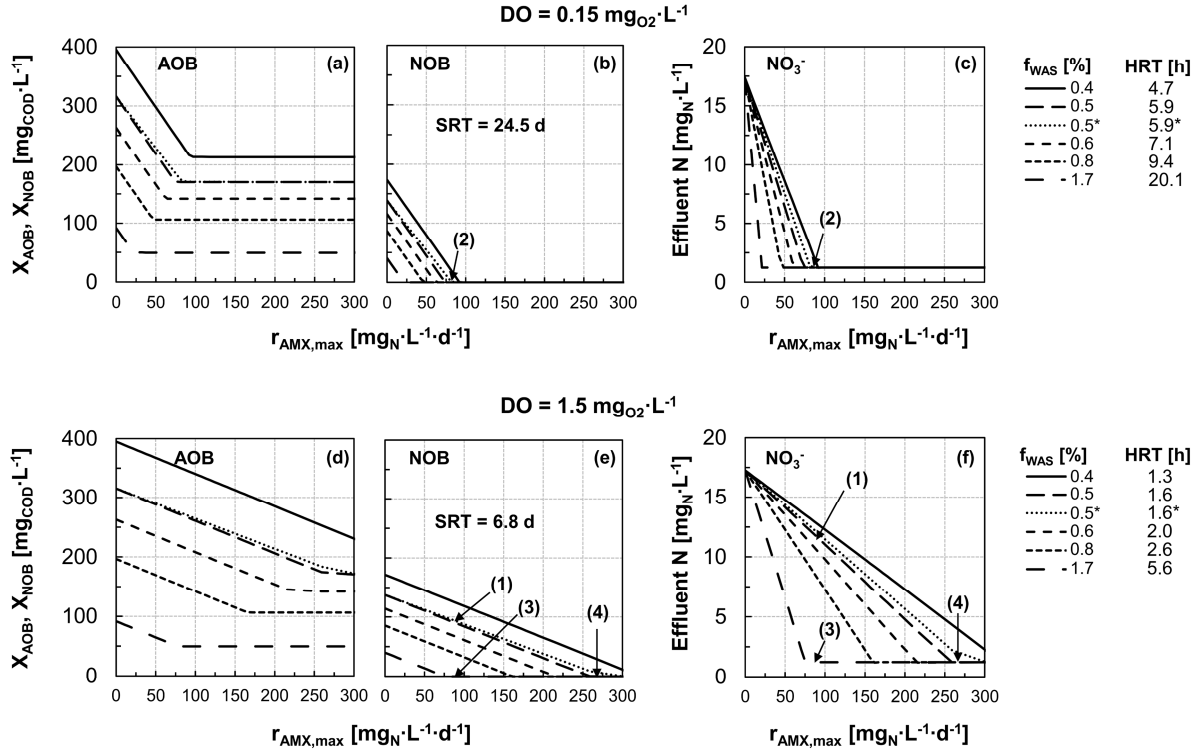
Scenario	DO [$\text{mg}_{\text{O}_2}\cdot\text{L}^{-1}$]	f_{WAS} [%]	$r_{\text{AMX,max}}$ [$\text{mg}_{\text{N}}\cdot\text{L}^{-1}\cdot\text{d}^{-1}$]
1 (baseline)	1.5	0.5	86
2	0.15	0.5	86
3	1.5	1.7	86
4	1.5	0.5	270

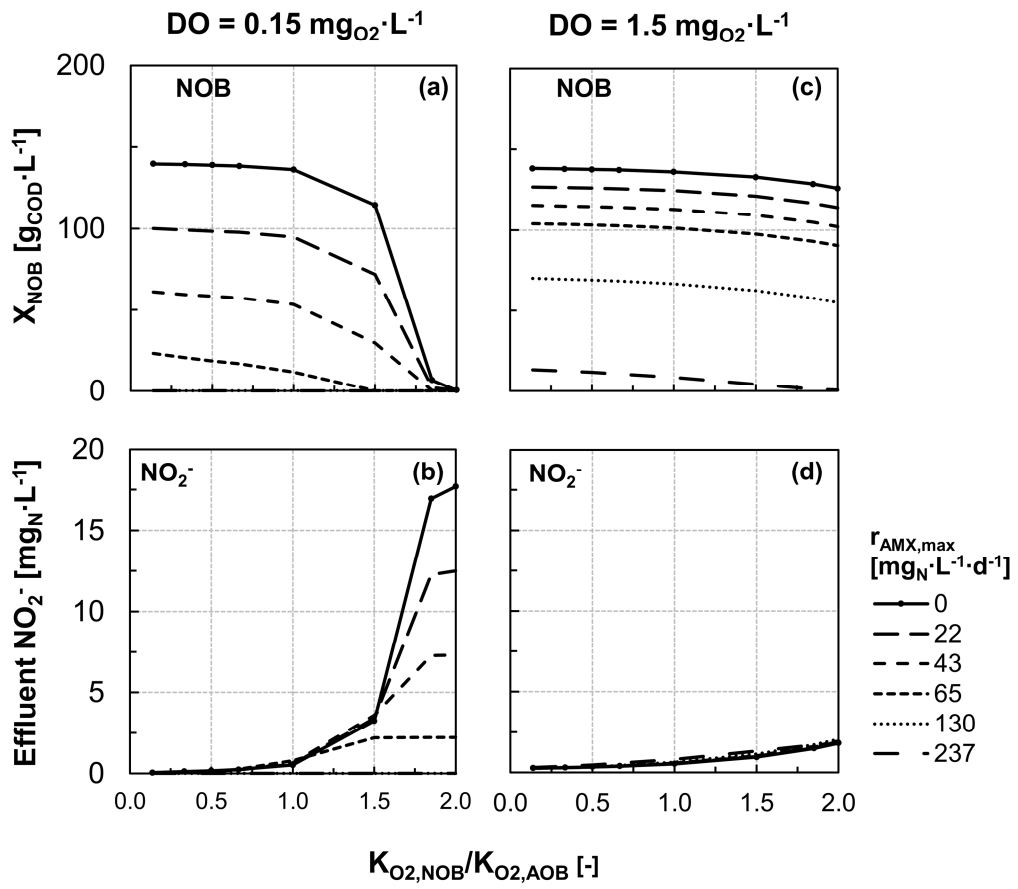












Highlights

- Hybrid PN/A systems provide increased operational flexibility for NOB control
- AOB and NOB enrich primarily in the flocs, and AMX in the biofilm (“NO₂-sink”)
- AMX use NO₂⁻ allowing to differentiate AOB and NOB growth rates
- A decrease in DO or an increase in floc removal leads to selective NOB washout from flocs
- The activity of the minor NOB fraction in the biofilm is suppressed at limiting DO